Biomaterials Advances 154 (2023) 213583

Contents lists available at ScienceDirect

Biomaterials Advances

journal homepage: www.journals.elsevier.com/materials-science-and-engineering-c

The ad hoc chemical design of random PBS-based copolymers influences the activation of cardiac differentiation while altering the HYPPO pathway target genes in hiPSCs

Giulia Guidotti [a], Robin Duelen [b], Nora Bloise [c,d], Michelina Soccio [a], Massimo Gazzano [e], Annalisa Aluigi [f], Livia Visai [c,d], Maurilio Sampaolesi [b,g,*], Nadia Lotti [a,**]

[a] Department of Civil, Chemical, Environmental and Materials Engineering, University of Bologna, Via Terracini 28, 40131 Bologna, Italy
[b] Translational Cardiomyology Laboratory, Stem Cell Biology and Embryology, Department of Development and Regeneration, KU Leuven, Leuven, Belgium
[c] Department of Molecular Medicine, Centre for Health Technologies (CHT), INSTM UdR of Pavia, University of Pavia, Viale Taramelli 3/B, 27100 Pavia, Italy
[d] Medicina Clinica-Specialistica, UOR5 Laboratorio di Nanotecnologie, ICS Maugeri, IRCCS, Via Salvatore Maugeri 4, 27100 Pavia, Italy
[e] Organic Synthesis and Photoreactivity Institute, CNR, Via Gobetti 101, 40129 Bologna, Italy
[f] Department of Biomolecular Sciences, University of Urbino Carlo Bo, Piazza del Rinascimento, 6, 61029 Urbino, (PU), Italy
[g] Histology and Medical Embryology Unit, Department of Anatomy, Histology, Forensic Medicine and Orthopedics, Sapienza University of Rome, Rome, Italy

ARTICLE INFO

Keywords:
Aliphatic polyesters
Poly(butylene succinate)
Electrospun scaffolds
Human induced pluripotent stem cells
Cardiac differentiation
HYPPO pathway

ABSTRACT

Cardiac tissue engineering is a cutting-edge technology aiming to replace irreversibly damaged cardiac tissue and restore contractile functionality. However, cardiac tissue engineering porous and perfusable scaffolds to enable oxygen supply in vitro and eventually promote angiogenesis in vivo are still desirable. Two fully-aliphatic random copolymers of poly(butylene succinate) (PBS), poly(butylene succinate/Pripol), P(BSBPripol), and poly(butylene/neopentyl glycol succinate), P(BSNS), containing two different subunits, neopentyl glycol and Pripol 1009, were successfully synthesized and then electrospun in tridimentional fibrous mats. The copolymers show different thermal and mechanical behaviours as result of their chemical structure. In particular, copolymerization led to a reduction in crystallinity and consequently PBS stiffness, reaching values of elastic modulus very close to those of soft tissues. Then, to check the biological suitability, human induced Pluripotent Stem Cells (hiPSCs) were directly seeded on both PBS-based copolymeric scaffolds. The results confirmed the ability of both the scaffolds to sustain cell viability and to maintain their stemness during cell expansion. Furthermore, gene expression and immunofluorescence analysis showed that P(BSBPripol) scaffold promoted an upregulation of the early cardiac progenitor and later-stage markers with a simultaneously upregulation of HYPPO pathway gene expression, crucial for mechanosensing of cardiac progenitor cells. These results suggest that the correct ad-hoc chemical design and, in turn, the mechanical properties of the matrix, such as substrate stiffness, together with surface porosity, play a critical role in regulating the behaviour of cardiac progenitors, which ultimately offers valuable insights into the development of novel bio-inspired scaffolds for cardiac tissue regeneration.

1. Introduction

Tissue engineering is an innovative interdisciplinary field and one in which there has been a dramatic increase in interest during the last decades, since it offers effective solutions for the treatment of many different diseases like cancer, diabetes, skin burns, and trauma [1,2]. Indeed, although pharmacological therapies are still the easier and most practiced approaches, in many cases they are not the most effective. This is particularly true for cardiovascular diseases (CVDs), one of the main causes of death and morbidity worldwide: myocardial infarction (MI) is the most serious CVD, which, if not lethal, results in the irreversible disfunction or loss of cardiomyocytes and functional tissue. Since adult cardiomyocytes lack the ability to self-regenerate, damaged tissue is replaced by a collagen-rich fibrotic substitute which is not able to

* Correspondence to: M. Sampaolesi, Translational Cardiomyology Laboratory, Stem Cell Biology and Embryology, Department of Development and Regeneration, KU Leuven, Leuven, Belgium.
** Corresponding author.
E-mail addresses: maurilio.sampaolesi@kuleuven.be (M. Sampaolesi), nadia.lotti@unibo.it (N. Lotti).

https://doi.org/10.1016/j.bioadv.2023.213583
Received 22 April 2023; Received in revised form 23 July 2023; Accepted 7 August 2023
Available online 12 August 2023

provide normal heart function and which, as a consequence, often leads to heart failure or arrhythmias [3,4]. Until recently, drug-supported transplantation was the only solution (with some serious drawbacks related to lack of donors and possible rejection). Nowadays, the advancements in the field of regenerative medicine are investigating new possibilities to overcome the inability of myocardium to regenerate by artificially recreating cardiac tissue with the ability to mimic normal function. Once properly developed, this new functional tissue could be implanted to replace damaged one: this process involves seeding the proper cell line on 3D porous supports, called scaffolds, which let cells grow, spread, proliferate and develop their extracellular matrix (ECM) [5,6]. Scaffolds with high porosity [7] and a proper cell morphology [8,9] can be fabricated by electrospinning, a common, cost effective and reproducible technique. These functional cardiac patches, once realized in vitro, can be potentially implanted directly onto the damaged tissue, improving cardiac function [7]. Indeed, it has been demonstrated that mechanical properties (in particular Young's modulus and surface stiffness) and topography (fibre alignment and dimension) can have a remarkable effect on cell adhesion and proliferation [8–11].

Polymeric biomaterials, such as aliphatic polyesters, are definitely the most interesting for the fabrication of scaffolds, offering a wide plethora of chemical and physic/mechanical properties, tunable in relation to the intended application. Among polymers, aliphatic polyesters are characterized by great versatility, combined with biodegradability and biocompatibility: necessary requirements for biomedical applications [7,12]. Poly(butylene succinate) (PBS), is an aliphatic polyester which has recently attracted considerable attention in biomedicine [13], due to its wide processing window, interesting mechanical properties and proven biocompatibility. It is acknowledged however that high crystallinity and rigidity limit its use in the field of soft tissue engineering. In order to exceed these limits, copolymerization, blending and the realization of nanocomposites are some of the strategies used, as reflected in the bibliography and in our previously published work [14–25].

As to the cell lines which can be used to evaluate the biocompatibility, stem cells are particularly interesting, due to their capability to maintain their pluripotency, boosting at the same time tissue growth. Among them, human-induced pluripotent stem cells (hiPSCs), commonly obtained by reprogramming adult somatic cells, have the same capability as all stem cells, but, unlike embryonic ones, are not subject to ethical or immunological challenges [3,26,27].

Previous studies have demonstrated that hiPSCs can be differentiated into cardiac progenitors and cardiomyocytes [26] but, to the best of our knowledge, cardiac differentiation on PBS-based scaffolds, starting from hiPSCs, has not been investigated yet.

Taking into account all these considerations, the present study reports on the synthesis and characterization of new PBS-based random copolymers designed for applications in cardiac tissue engineering. Two different comonomers were chosen, neopentyl glycol (a glycol characterized by short ramifications along its main chain) and Pripol 1009 (a fatty acid containing an aliphatic 6 carbon atoms ring and PE-like moieties along the main chain, together with long side chains). The different chemical structure of the two comonomers was expected to result in different solid-state and functional properties of the final materials: as is well known, side long alkyl groups increase flexibility, reducing the crystallizing ability, while an opposite effect is observed when short alkyl groups are present [28–30]. Electrospun scaffolds were obtained from the two copolymers and their biocompatibility was tested using hiPSCs. After a preliminary biocompatibility evaluation, carried out by cell viability, we examined the PBS-based scaffolds effects on gene expression of some pluripotency markers. Analysis included the expression of integrins, which have been demonstrated to play a key role in adhesion and proliferation of stem cells on substrates [31,32], and the HIPPO pathway, which has an important impact on stem cell proliferation, self-renewal, and differentiation [33,34]. Finally, iPSCs were differentiated into cardiomyocytes on PBS-based scaffolds and early and late cardiac markers were investigated.

2. Experimental methods

2.1. Materials

Dimetyl succinate (DMS), 1,4-butanediol (BD), neopentyl glycol (NG), titanium tetrabutoxide (TBT) were purchased from Merck and used as reagent-grade. Pripol 1009 is a commercial biobased diacid kindly provided by Croda.

2.2. Polymer synthesis

Poly(butylene succinate/Pripol) P(BSBPripol) and poly(butylene/neopentyl glycol succinate) P(BSNS) were synthesized according to two-step melt polycondensation, as previously reported [30,35]. The synthetic apparatus consisted of a glass reactor, put in a thermostated sodium salt bath, a mechanical stirrer connected to a torque measurer and a high vacuum pump. Different molar amounts of DMS and Pripol1009 in the former case, and BD and NG in the latter were placed in the reactor, to obtain final polymers with a 70 mol% of BS units, together with the catalysts TBT (200 ppm). A small glycol excess (30 mol%) was used. During the first step, which lasted about 90 min, the temperature was set at 180 °C and the reaction carried out under stirring (100 rpm) and inert nitrogen atmosphere. During this phase, transesterification (in case of P(BSNS)) and esterification (in case of P(BSBPripol)) reactions occurred, together with distillation of methanol or water, respectively. Then, the second step started by gradually reducing the pressure to 0.1 mbar and raising the temperature to 220 °C. In this phase, transesterification reactions and removal of glycolic excess occurred, resulting in an increase of polymeric fluid viscosity (i.e. of molecular weight), monitored by torque measurement. After circa four additional hours, when the torque had reached a constant value, the synthesis was stopped and the obtained polymer was purified by dissolution in chloroform and further precipitation in cold methanol.

2.3. Molecular characterization

The chemical structure and the composition of the synthesized samples was determined by proton Nuclear Magnetic Resonance (^{1}H NMR). The solutions of the two copolymers solved in deuterated chloroform (containing tetramethylsilane as an internal standard) were analysed using a Varian INOVA 400 MHz apparatus at room temperature (64 scans, relaxation delay of 0 s and acquisition time of 1 s).

Molecular weight and polydispersity index were calculated through gel permeation chromatography (GPC), carried out at 30 °C. The apparatus, a Hewlett Packard instrument, is equipped with a PL gel 5 m MiniMIX-C column and a refractive index detector, and calibrated using monodisperse polystyrene standards in the range of 2000–100,000 Da. Samples were solved in chloroform, used also as eluent (0.3 ml/min), at a concentration of about 2 mg /ml.

2.4. Film and scaffold preparation

Polymeric films (of about 100 μm thickness) were obtained by compression moulding, using a Carver C12 Laboratory press, equipped with a cooling apparatus. 1.5 g of material was put between two Teflon sheets and melted. Then, a pressure of about 5 ton/m^2 was applied for two minutes. Films were cooled ballistically in press, until room temperature was reached, and then stored at this temperature for three weeks, to let them reach thermal equilibrium.

Fibrous scaffolds were obtained by electrospinning. Polymeric solutions were prepared by solving 600 mg of polymer in 4 ml of 1,1,1,3,3,3-hexafluoro-2-propanol. The apparatus used consisted of a syringe, with a needle having an internal diameter of 0.8 mm and connected to a voltage generator (20 kV), a metallic collector (0 V, working

distance of 15 cm) and a pump for the injection. Each solution was charged in the needle and injected with a flow rate of 1.8 ml/h.

2.5. Morphological characterization of scaffolds

The fibrous electrospun scaffold morphology was observed through a desktop Phenom scanning electron microscope (SEM). Before the analysis, samples were metal sputtered and glued on aluminium stabs. For the measurement of the fibre diameter, GIMP 2.8 (GNU Image Manipulation Program) software was employed, and 200 fibres, randomly collected from different SEM images, were analysed.

2.6. Thermal and structural characterization

Thermal stability was determined by means of thermogravimetric analysis (TGA), using a TGA4000 (Perkin Elmer) instrument. Polymeric samples were loaded on a weight scale and heated at constant rate of 10 °C/min from 40 to 800 °C under inert atmosphere. T_{onset} and T_{max}, i.e. the temperature at which weight loss starts and the temperature corresponding to maximum weight loss, respectively, were measured.

Differential scanning calorimetry (DSC) was carried out to determine polymer thermal transitions, by means of a DSC6 (Perkin Elmer) instrument. The typical setup consists of an intracooler set at −70 °C and a holder, containing both the sample and the reference, kept under nitrogen atmosphere. The calorimetric program was the following: I scan from −50 °C to 150 °C (heating rate of 20 °C/min) followed by an isothermal step of 3 min, a rapid cooling from the molten state at a rate of 100 °C/min, followed by an isothermal step of 15 min, and then a II heating scan, under the same conditions. Thermal transition temperatures as well as the corresponding heats, i.e. glass to rubber transition (T_g), melting temperature (T_m) and their relative specific heat and enthalpy variations (Δc_p and ΔH_m, respectively) were calculated.

The kind and amount of crystalline phases were determined by means of wide-angle X-Ray scattering (WAXS), with a PANalytical X'Pert PRO diffractometer equipped with an X'Celerator detector and a copper target. Data were acquired at room temperature in the 5–60° 2θ range (acquisition time of 100 s; step of 0.10°). Crystallinity degree (X_c) was determined as the ratio between the crystalline peak area and the overall area under the diffractometric curve, also considering non-coherent scattering.

2.7. Mechanical characterization

Mechanical testing was carried out using an Instron 5966 machine, equipped with rubber grips and a 10 kN load cell controlled by a Bluehill software. Polymeric specimens (5 mm × 50 mm, gauge length of 20 mm) were first subjected to tensile tests, with a stretching speed of 10 mm/min. At least 6 samples for each experiment were analysed. The load-displacement data have been converted to stress−strain curves. Stress (σ_B) and elongation (ε_B) at break were directly measured, while the tensile elastic modulus (E) was determined from the initial linear slope. Cyclic loading analysis was then performed: samples were strained at a strain well below their percentage deformation at break (about 45–50 %), and then 25 cycles at the rate of 10 mm/min were carried out.

2.8. Wettability and hydrolytic degradation tests

Static water contact angle (WCA) measurements were performed at 23 °C on polymeric films and scaffolds by means of a KSV CAM101 instrument equipped with Drop Shape Analysis software. The profiles of 8 deionized water drops (volume of 4 μl) were recorded and analysed immediately after deposition on different surface areas of each sample. WCA values were reported as the average value ± standard deviation.

Hydrolytic biodegradation tests were performed by incubating polymeric samples, previously weighted, in phosphate saline buffer (0.1 M, pH 7.4) at 37 °C under agitation (50 rpm) using a SW22 Julabo shaking water bath. The buffer solution was changed weekly to keep the pH constant during the entire experiment. At designated time points, specimen duplicates were withdrawn, washed repeatedly with water and then dried under vacuum until a constant weight was reached. Gravimetric weight loss was determined by dividing the difference between the initial and final weight of each sample by the initial one and molecular weight loss was evaluated through GPC analysis.

2.9. Cell culture

Commercially available integration-free human iPSC line (Thermo Fisher Scientific), generated using cord blood-derived $CD34^+$ progenitors with seven episomally expressed factors (OCT4, SOX2, KLF4, c-MYC, NANOG, LIN28 and SV40 T) were cultured, and maintained in feeder-free condition in a 6-well culture plate with Geltrex™ LDEV-Free (hESC-Qualified, Reduced Growth Factor Basement Membrane Matrix, Thermo Fisher Scientific) in Essential 8™ medium (Thermo Fisher Scientific) under normoxic conditions (37 °C, 5 % CO_2). Cells were passaged non-enzymatically in colonies using EDTA (Thermo Fisher Scientific) every 4–6 days with daily medium changes. Two different studies were performed: assessing biocompatibility and cardiac differentiation. Prior to cell seeding, P(BSNS) and P(BSBPripol) were cut in round shaped pieces (area of 4 cm^2, about 150 μm thick) and assembled in 12 CellCrown supports (Scaffdex, Tampere, Finland) in order to prevent them floating in the cell culture medium. The samples were sterilized with decreasing concentrations of ethanol (96- and 70 %) for 15 min each, washed twice in 1× phosphate-buffered saline (PBS) for 10 min, assembled in the well plates, and then incubated overnight with Essential 8™ medium at 37 °C.

2.10. hiPSCs viability

To assess scaffold biocompatibility, hiPSCs cell colonies were dissociated and seeded at a density of 1×10^5 cells per cm^2 on the top of P(BSNS) and P(BSBPripol) treated or not treated with Geltrex™, in Essential 8™ medium, and incubated at 37 °C with 5 % CO_2. In parallel, cells were cultured on Geltrex-Tissue Culture Plates (TCPS-GTX) for use as positive control. The culture was maintained up to 6 days with a daily medium exchange. At 6 days of culture, cell viability, morphology and pluripotency were evaluated. The hiPSC viability on the different substrates was evaluated at day 1 and at day 6 (the end of culture period) after seeding by 3-[4,5-dimethylthiazol-2-yl]-2,5 diphenyl tetrazolium bromide assay (MTT assay, Sigma-Aldrich, St Louis, MO, USA). Each substrate was transferred into a 12-well culture plate and the medium was replaced by 500 μl of DMEM medium, followed by the addition of 50 μl of MTT reagent (5 mg ml^{-1}) as previously described [36]. The substrate were then incubated for 4 h at 37 °C in a humidified 5 % CO_2 incubator. Formazan crystals, formed by the interaction of the MTT solution with the live cells, were then dissolved in 1: 1 (*v*/v) isopropanol - 0.04 M HCl. Aliquots of 100 μl were sampled and the absorbance was measured at 565 nm by using a microplate reader (BioRad Laboratories, Hercules, CA). A standard curve of cell viability was used to express the results as percentage viable cells in comparison with TCPS-GTX.

2.11. Cardiac differentiation

Human iPSCs were differentiated into functional cardiomyocytes (CMs) according to a monolayer-based protocol (Scheme 1) from Life Technologies (PSC Cardiomyocyte Differentiation Kit Prototype). Briefly, hiPSCs were seeded on the top of P(BSNS) and P(BSBPripol) scaffolds, previously sterilized, inserted into a 12-well culture plate and coated with Geltrex™ at a low initial density (splitting ratio 1:20) in an Essential 8™ medium under hypoxic conditions (37 °C, 5 % CO_2, 5 % O_2). At day 0 of differentiation, cells were placed under normoxic conditions and differentiated towards the mesodermal lineage. This was done with a chemically defined medium consisting of RPMI 1640

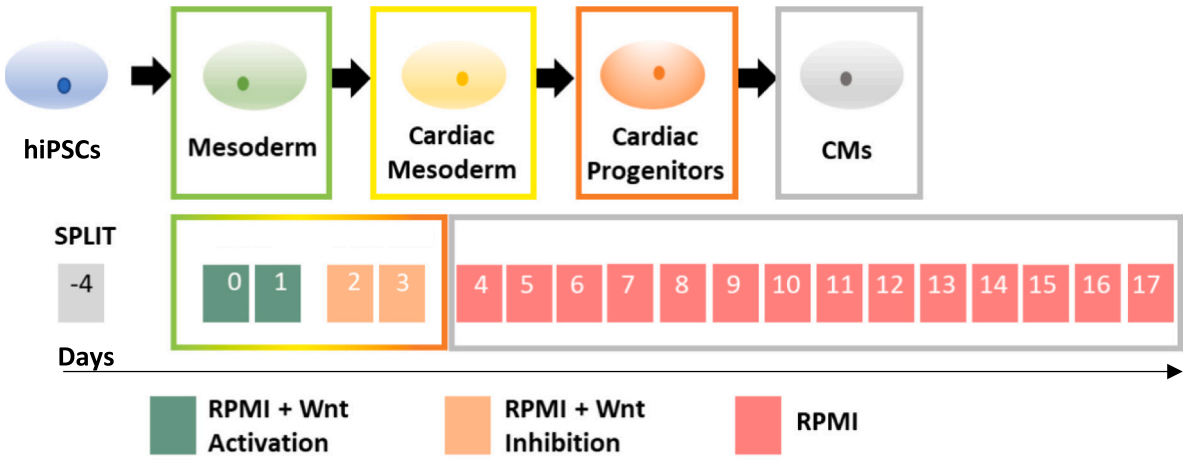

Scheme 1. Schematic representation of the monolayer-based cardiac differentiation protocol, from hiPSCs to cardiomyocytes (CMs) using RPMI 1640 medium added first with a Wnt activator for mesoderm differentiation (days 0–1), and then with a Wnt inhibitor to obtain cardiac progenitors (days 2–3). From day 4 onwards only RPMI was used to feed the cells.

(Thermo Fisher Scientific), supplemented with 5 to 7 μM CHIR99021 (Wnt activator, GSK3β inhibitor; Axon Medchem) for 48 h (Cardiomyocyte Differentiation Medium A). At day 2, the mesodermal cells were fed with a basal medium containing 4 μM IWR-1 (Wnt inhibitor; Merck) for 48 h (Cardiomyocyte Differentiation Medium B). From day 4 onwards, the medium was changed every two days with Cardiomyocyte Maintenance Medium. Cells cultured in GTX-coated TCPS (6-well culture plate) were used as a positive control.

2.12. Quantitative real-time PCR (RT-qPCR)

Total RNA from human iPSCs seeded on scaffolds and control conditions was extracted using the PureLink RNA Mini Kit (Thermo Fisher Scientific) and treated with the DNA-Free Kit (Thermo Fisher Scientific) to obtain highly pure RNA. 250–500 ng RNA was reverse transcribed into cDNA with Superscript III Reverse Transcriptase First-Strand Synthesis SuperMix (Thermo Fisher Scientific). Quantitative real-time PCR was performed with the Platinum SYBR Green QPCR SuperMix-UDG (Thermo Fisher Scientific), using ViiA7 Real-Time PCR instrument (Applied Biosystems). The oligonucleotide primer sequences are reported in Table S2 (from IDT). A 10-fold dilution series ranging from 10^{-3} to 10^{-8} of 50 ng/μl human genomic DNA was used to evaluate the primer efficiency. Gene expression was analysed in triplicate and normalized to the CT mean of housekeeping genes (*GAPDH, RPL13a* and *HPRT*) expression using the ΔΔCt Livak method.

2.13. Immunofluorescence

For indirect immunofluorescence, samples were washed with PBS, fixed 20 min with 4 % (*w/v*) paraformaldehyde solution (PFA; Polysciences) at 4 °C. Subsequently, the fixed cells were permeabilized with 0.2 % Triton X-100 in 1 % bovine serum albumin (BSA, Merck) and blocked with 10 % Donkey Normal Serum (Merck) for 30 min at room temperature. For pluripotency factor labelling, hiPSCs-seeded scaffolds sampled at 6 d of culture were incubated overnight at 4 °C in a humid atmosphere with primary goat antibody anti-octamer-binding transcription factor 4 (OCT4, 5 μg/ml, Santa Cruz SC-8626, Dallas, TX, USA) and primary rabbit antibody anti-NANOG (10 μg/ml, Thermo Scientific PA1-097×). After washing with PBS, samples were incubated 1 h at room temperature with Alexa Fluor 488- and 594-conjugated secondary antibodies (Thermo Fisher Scientific 4 μg/ml). In all studies, parallel negative controls (without primary antibody material) were undertaken. For cardiomyocytes differentiation, fixed hiPSCs-seeded scaffolds sampled at 7 d of differentiation, were incubated with primary antibody mouse anti-Actinin Alpha 2 (ACTN2, 5 μg/ml, Abcam EA-53;) and goat anti-NKX-2.5 (5 μg/ml, Santa Cruz Biotechnology A-16). For both types of evaluations, after extensive washes with PBS, hiPSCs-scaffolds were incubated 1 min with Hoechst 33342 for nuclei staining (diluted 1:10000 in PBS, Thermo Fisher Scientific). Images were acquired using a ZEISS LSM800 confocal microscope (ZEISS) and an Eclipse Ti Microscope and NIS-Elements AR 4.11 Software (Nikon, Japan).

2.14. Statistical analysis

All the experiments were performed technically in triplicate and at least two/three independent experiments. The results were represented as mean ± Standard Deviation (SD). All statistical analyses were carried out using GraphPad Prism 6.0 (GraphPad Inc., San Diego, CA). Analysis was performed using one-way and two-ways analysis of variance (ANOVA), followed by Bonferroni post hoc test (significance level of 0.05).

3. Results and discussion

3.1. Synthesis and molecular characterization of PBS-based copolymers

In the present paper, two random copolymers (P(BSBPripol) and P(BSNS)) of poly(butylene succinate) with similar composition were prepared in melt by polycondensation using $Ti(OBu)_4$ (TBT) as biocompatible catalyst. The copolymer composition was kept constant, in order to correlate the final polymer properties with the different chemical structure of the comonomeric unit introduced in PBS backbone. In case of P(BSBPripol), we introduced a bulky co-unit characterized by high flexibility, imparted by the long PE-like ramifications. In the other case, (P(BSNS)), short ramifications were inserted along PBS macromolecular chain.

As is known, the presence of alkyl pendant groups usually hinders rotation around the C—C σ bond because of their high steric hindrance, which reduces the macromolecular mobility (T_g increases). However, in the case of pendant groups which are sufficiently long, an internal plasticizing effect prevails, leading to a decrement of the T_g value. The entity of the effect is proportional to the length of the side alkyl group. Considering this general trend, it was expected that the Pripol containing co-unit would exert a predominantly elastic effect in contrast to the NS, which should render the final polymer more rigid.

The as-prepared samples were first characterized from the molecular point of view by means of ^{1}H NMR spectroscopy and GPC analyses. The molecular characterization data are collected in Table S1, while in

Fig. S1 the ^{1}H NMR spectra of the two copolymers are shown.

As shown by Fig. S1A, all the peaks of BS co-unit are present, being the *a* and *b* methylene protons of the butylene subunit located at δ 4.2 ppm and δ 1.7 ppm, respectively, while the singlet *c* of the acid subunit is situated at δ 2.6 ppm. As to the peaks of the BPripol subunit, the methylene protons, *d* and *e* of the glycol subunit are located at δ 4.2 ppm and δ 1.6 ppm, respectively, while the triplet *f* of the protons related to the acid subunit in α position with respect to the carboxylic group appeared at δ 2.3 ppm. At lower chemical shifts (1.5 ppm < δ < 0.7 ppm) the signals of R subunit of Pripol *g*, *h*, *i* and *j* can be seen. Also for P (BSNS) sample (Fig. S1B), all the peaks of BS counit are present (*a* and *b* protons of butylene subunit at δ 3.9 ppm and δ 1.68 ppm, respectively, as well as the singlet *c* of the acid subunit at δ 2.6 ppm), together with the peaks related to NS comonomeric unit: *d* and *e* singlets associated with neopentyl glycol are located at δ 4.1 ppm and δ 0.95 ppm, respectively, while the singlet *f* of the acid subunit can be found at δ 2.65 ppm.

The effective chemical composition of P(BSBPripol) copolymer was calculated from the relative area of *f* methylene protons of Pripol subunit at δ 2.3 ppm, and the relative area of *c* protons of succinic subunit at δ 2.6 ppm. In the case of P(BSNS), we considered the relative area of *d* protons of neopentyl glycol subunit at δ 4.1 ppm and the relative area of *c* protons of succinic subunit at δ 2.6 ppm, respectively. For both samples, the molar amount of BS comonomeric unit turned out to be very close to the feed one. Moreover, the two copolymers are characterized by similar molar composition, BS molar amount being 60 % in case of P(BSBPripol) and 65 % for P(BSNS).

Molecular weight obtained by GPC were both high and characterized by a quite low polydispersity index, suggesting a good control over polycondensation reactions (Table S1).

3.2. Morphological, thermal and mechanical properties of PBS-based films and scaffolds

3.2.1. Morphologic characterization of scaffolds

In Fig. 1, SEM pictures of P(BSNS) and P(BSBPripol) nanofibrous scaffolds are shown at two different magnifications (20× and 50× magnifications). As can be seen, no beads are present, demonstrating the effectiveness of the electrospinning procedure. As a matter of fact, the development of crystallinity during solvent evaporation avoids the formation of agglomerates and so provide structural strength to the fibres. As can be seen from distribution graph, the fibres present quite different diameters. This is because of the jet-splitting phenomena, which starts from the primary jet and causes secondary jets of smaller dimensions. In all the samples analysed, the fibres are characterized by a non-Gaussian distribution, probably due to this jet-splitting phenomena, with dimensions ranging between 100 and 1100 nm in the case of P(BSNS) and 100 to1800 nm for the P(BSBPripol).

3.2.2. Thermal characterization

Both films and scaffolds obtained from the synthesized polymers have been subjected to thermogravimetric analysis under dry nitrogen atmosphere. The temperature corresponding to the beginning of degradation (T_{onset}) and to the maximum rate of decomposition (T_{max}) are listed in Table 1, while the corresponding thermogravimetric curves are reported in Fig. S2. All the samples under investigation show a very good thermal stability (T_{onset} above 380 °C). Copolymerization slightly improves the thermal stability of PBS, the effect being more evident when the Pripol containing co-unit is present, probably due to a lower density of carboxylic groups inside the macromolecular chains [30]. In case of P(BSNS), the improvement of thermal stability can be ascribed to the presence in the glycol subunit of NS co-unit of two methylene groups in place of hydrogen atoms, which prevent β scission reactions [37,38],

It has also to be noticed that electrospinning process does not affect the thermal stability of the materials under study, as the scaffolds do not show any difference in terms of T_{onset} and T_{max} with respect to films.

Calorimetric analysis of all films and scaffolds was performed after three weeks of storage at room temperature, to standardise the thermal history of the samples. I scan calorimetric data are collected in Table 1, while in Fig. 2 I scan traces are shown, together with those of PBS homopolymer, added for sake of comparison. The DSC trace of both PBS parent homopolymer film and scaffold is typical of a semicrystalline material, showing a glass transition phenomenon (T_g = −35 °C), followed by a pronounced endothermic melting peak at 114 °C.

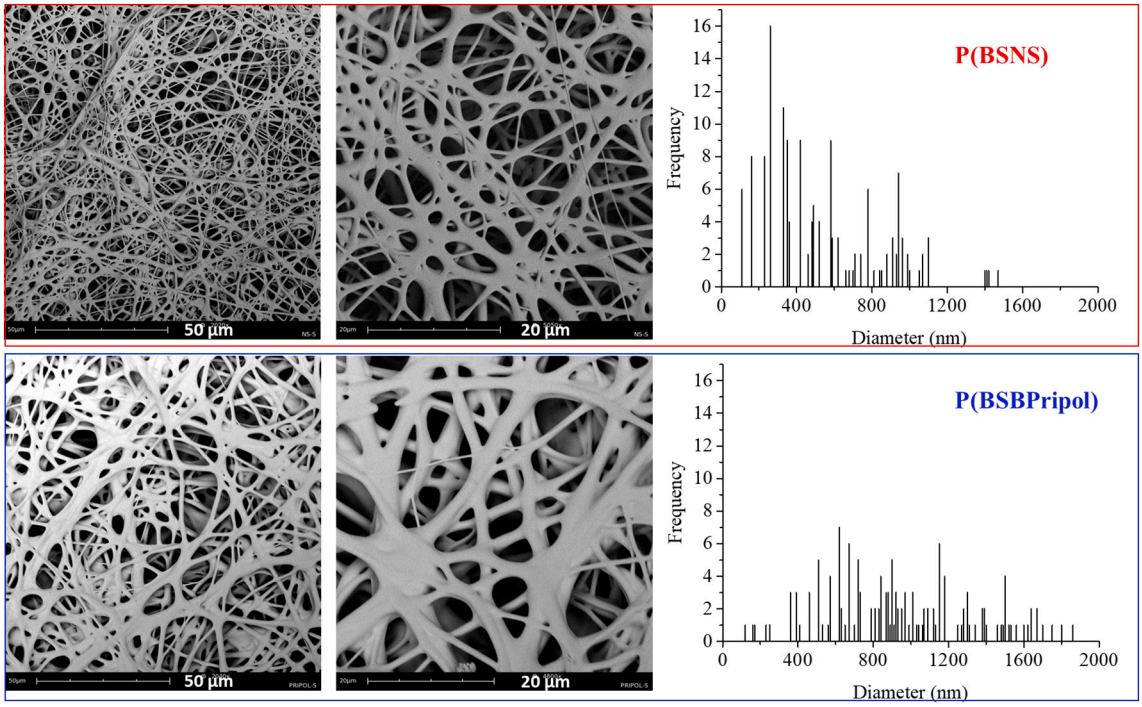

Fig. 1. SEM picture of P(BSNS) and P(BSBPripol) scaffolds, and fibres' diameter distribution.

Table 1
Thermal characterization data (DSC and TGA) and crystallinity indexes (WAXS) of PBS, P(BSNS) and P(BSBPripol) films and scaffolds (*).

Polymer	T_{onset} (°C)	T_{max} (°C)	I SCAN				Xc (%)
			T_g (°C)	ΔC_p (J/g °C)	T_m (°C)	ΔH_m (J/g)	
PBS[a]	385	407	−35	0.088	114	50	46
P(BSNS)	384	415	−28	0.244	42 77	33	31
P(BSBPripol)	391	426	−50	0.194	42 65	21	14
PBS*	363	398	−32	0.193	114	64	41
P(BSNS)*	362	401	−28	0.267	44 72	40	39
P(BSBPripol)*	386	421	−51	0.192	47 64	23	20

[a] Ref. [35].

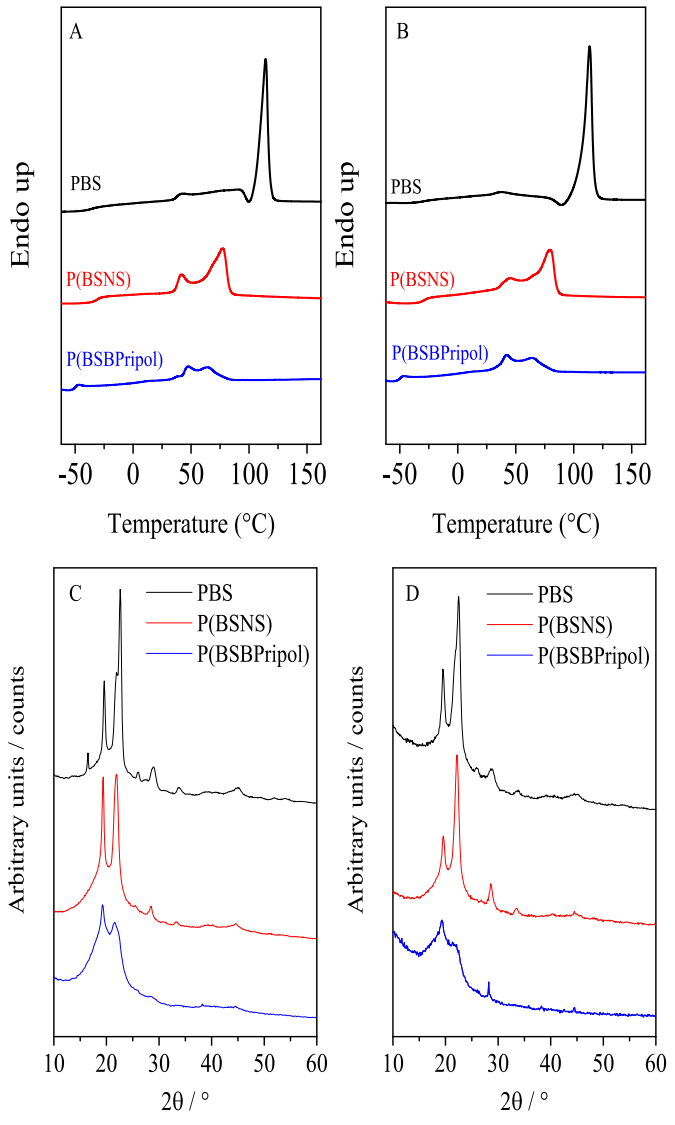

Fig. 2. I scan calorimetric curves of PBS, P(BSNS) and P(BSBPripol) in form of films (A) and scaffolds (B) (20 °C /min); X-Ray diffraction profiles of PBS, P (BSNS) and P(BSBPripol) in form of films (C) and scaffolds (D).

Copolymerization deeply affects both T_g and T_m values: more in detail, the P(BSBPripol) sample is characterized by a lower T_g and by a higher ΔC_p values with respect to PBS homopolymer. The T_g decrement can be ascribed to the plasticizing effect of the long aliphatic segments present in Pripol moiety. Conversely, the presence of the short alkyl side groups in P(BSNS), is responsible for an increase of T_g value, because of the steric hindrance effect, which inhibits the rotation around the C—C σ bond. In this case, the ΔC_p value was also higher than that of the PBS, indicating a higher amorphous fraction in the copolymer. In addition, in both copolymers, the melting phenomenon occurs at lower temperature and is less intense (lower ΔH_m value) when compared with the PBS homopolymer, indicating the introduction of comonomeric units along the PBS main chain deeply hampers the crystallization capability of BS segments. This behaviour, particularly pronounced in the P(BSBPripol) samples, can be explained as due to the formation in the copolymer of a smaller amount of crystalline phase, characterized by a lower degree of perfection. Last, but not least, the melting peak changes shape due to copolymerization: DSC trace of PBS shows a sharp single melting peak whereas in the case of copolymers, the endothermic process is wider and double. As is usually observed for polyesters [39–41], the double melting peak is due to the melting-crystallization-remelting phenomena, with crystals which melt and crystallize in a more perfect form during heating. A similar behaviour can be seen in the P(BSNS) samples, although in this case the T_m and ΔH_m values are higher than those found for the other copolymer, because of the presence of short ramifications which hinder to a lesser extent the crystallization capability of PBS. Indeed, as previously reported [35], NS co-units can be partially included in PBS crystalline lattice, supporting co-crystallization.

It should also be noted that electrospinning does not alter the thermal behaviour of the materials, the DSC profiles of scaffold being very similar to those of film (Fig. 2).

3.2.3. *Structural characterization*

To understand the nature and the amount of crystalline phase present in the copolymeric films and scaffolds under investigation, a WAXS analysis was performed. In Fig. 2 the diffraction profiles are shown and in Table 1 the values of crystallinity degree X_c are listed.

All the profiles obtained are typical of semicrystalline polymers, with well-defined peaks, overlapped to a bell-shape baseline characteristic of amorphous regions.

On the basis of the patterns obtained, all the samples that were analysed crystallized according to α-PBS crystal phase, no other crystal phases were present [42,43]. The main PBS lattice reflections, located at $2\theta = 19°$ and 23°, change in intensity by copolymerization. In P(BSNS) pattern as well as in the case of PBS the reflection at $2\theta = 23°$ was more intense than the peak at $2\theta = 19°$. For the P(BSBPripol) samples we observed the opposite. It can be hypothesized that in P(BSBPripol) a partial lattice distortion occurs. In this copolymer, peak position remains unchanged, proving that the Pripol containing co-units are excluded from the crystalline phase, and rejected in the amorphous one. On the contrary, with P(BSNS), a partial inclusion of the NS co-unit inside the PBS crystalline lattice takes place, as evidenced by an increasing in the cell volume [35]. The result is not surprising when we consider that the chemical structure of neopentyl glycol is not considerably different from that of butanediol found in PBS. Conversely, in the P(BSBPripol)

copolymer, the two diacid sub-units, i.e. Pripol diacid moiety and succinic acid, are extremely different. By comparing the X-Ray diffraction profiles of films, it is possible to observe that PBS is the most crystalline sample (X_c = 46 %), followed by P(BSNS) with the P(BSBPripol) copolymer being the least crystalline (Table 1). Not even this result is particularly surprising if we consider that in case of P(BSNS) co-crystallization occurs.

The results for the scaffold samples were analogous with those observed for the films. Lastly, the crystallinity indexes obtained from diffractometric analysis are consistent with the calorimetric data (Table 1).

3.2.4. Mechanical characterization

The tensile testing data (elastic modulus E, stress at break σ_B and strain at break ε_B) are summarized in Table 2. Stress-strain curves for PBS, P(BSBPripol) and P(BSNS) copolymers, in form of films and scaffolds, are shown in Fig. 3A and Fig. 3B, respectively, while in Fig. 3C cyclic loading curves for the same materials are reported.

Of all the films analysed, the PBS was the stiffest (highest elastic modulus value, of about 301 MPa) and most fragile (lowest elongation at break, of only 5 %). The film prepared from random PBSP(BPripol) copolymer shows a significant different mechanical behaviour with respect to PBS homopolymer, behaving like an elastomer with a low elastic modulus and a high elongation at break. Interestingly, although P(BSBPripol) is a random copolymer, the stress-strain curve of film does not show any yield (Fig. 3A), probably because of the bulky size of Pripol co-units, which determines a sort of block structure within the copolymer. The P(BSNS) film has elastic modulus and a stress breaking point which is very similar to the PBS samples, though the elongation at break being significantly higher (219 % vs. 5 %). Moreover, the presence of yielding is recorded. The measured stress strain curve is typical of a material with a plastic behaviour, i.e. high strength, high ductility, high toughness. The presence -CH_3 side group, as already mentioned, is responsible of two effects, the decreasing of crystallinity degree, and the increasing of chain rigidity. The results obtained indicate the latter factor prevails on the former.

By comparing the mechanical response of the two copolymers, it is possible to see how Pripol-containing film is characterized by lower E (more than one order of magnitude) and σ_B (almost one order of magnitude) and greater elongation (460 % vs. 219 %). This trend must be ascribed to the higher crystallinity degree and the higher T_g value of P(BSNS).

The mechanical response of the scaffolds was different (Fig. 3B). In particular, PBS and P(BSNS) scaffolds exhibit similar elastic modules, stress and elongate at break, at a rate which is even slightly higher for PBS scaffold (≈23 %). This result can be explained by the similar crystallinity degree for the two samples. The P(BSBPripol) scaffold is instead characterized by a halved elastic modulus but exhibited similar stress at break and elongation characteristics, again due to the lower crystallinity of this sample with respect to both PBS and P(BSNS). It is also interesting to note that the elastic modulus values of scaffolds are particularly low, considering the common mechanical properties of thermoplastic polymers, and makes these materials suitable for cardiac tissue engineering. Indeed, although the elastic modulus of cardiac muscle is in the range of kPa [44], previous studies reported in the literature have demonstrated that materials with E in the range 2–80 MPa successfully supported myocardial cells growth and proliferation [45–48]. Last, but not least, in the stress-strain curves of both P(BSBPripol) and P(BSNS) scaffold yield is not evident.

Cycling stress-strain measurements were carried out on P(BSNS) scaffold and on P(BSBPripol) film and scaffold samples to investigate the behaviour of the copolymers when subjected to cyclic stress (Fig. 3C). The P(BSNS) results indicated quite low levels of elasticity, the amount of permanent set remained at about 30 %. In addition, the hysteresis area of all the cycles is quite similar to that of the first cycle, indicating an incomplete energy recovery. The P(BSBPripol) copolymeric film possessed good levels elasticity, though the amount of permanent set was at about 22 %, after each loading–unloading cycle. In addition, the stress–strain curve in the second cycle was more compliant than that observed in the first cycle. This behaviour, known as softening, can be due to a rearrangement in the crystalline microphase [49]. Lastly, the hysteresis area of the second cycle is much smaller than that of the first cycle, thus indicating good energy recovery. The comparison between the performance of P(BSBPripol) film and scaffold after cyclic loading indicates the scaffold showed lower levels of elongation at breaking (Table 2 and Fig. 3C). That is largely because of the 3-dimensional porous structure, and the extent to which pores and defects determine the fracture of the sample at lower stress with respect to the film, although they are characterized by similar behaviours.

Table 2
Mechanical characterization data of PBS, P(BSBPripol) and P(BSNS) in form of films and scaffolds (*).

Polymer	σ_B (MPa)	ε_B (%)	E (MPa)
PBS	16 ± 2	5 ± 1	301 ± 25
P(BSNS)	18 ± 1.0	219 ± 12	340 ± 34
P(BSBPripol)	4.6 ± 0.3	460 ± 22	14 ± 2
PBS*	6 ± 1	151 ± 7	20 ± 3
P(BSNS)*	3 ± 0.5	116 ± 13	24 ± 5
P(BSBPripol)*	2 ± 0.3	134 ± 16	10 ± 3

3.2.5. Wettability and hydrolytic degradation tests of PBS-based films and scaffolds

Wettability of PBS-based films and scaffolds was evaluated by water contact angle (WCA) measurements. WCA values are listed in Table 3, while drops pictures are shown in Fig. S3. All the materials under study are hydrophobic (WCA > 90°), the hydrophobicity slightly increasing in P(BSBPripol) sample, due to the presence of long aliphatic segments in the main chain. By comparing films and scaffolds, the same trend can be observed, and the hydrophobic behaviour is even more evident.

Hydrolytic degradation experiments were carried out under physiological conditions. At predetermined time points sacrificial samples were collected and weighted, their molecular weight was calculated by means of GPC analysis. In addition, the samples were subjected to ^{1}H NMR, DSC and WAXS analyses, to assess the residual composition and possible differences in crystallinity degree.

As it is well known, hydrolysis is a bulk phenomenon: the macromolecular chains are attacked by water and consequently the molecular weight starts to decrease, as the hydrolysed chains are not able to solubilize during the first stages of degradation. For this reason, gravimetric weight loss is negligible and occurs only after longer times. In Table 3 both weight loss and molecular weight loss data after 15 weeks of incubation are reported together with calorimetric data for all the samples under investigation (films and scaffolds).

As regards the films, according to the data collected in Table 3, no appreciable weight losses were observed, the values ranging from 2 to 3 %. As to the corresponding scaffolds, slightly higher weight loss percentages were measured (around 5 %), because of the higher surface/volume ratio due to the nanofibrous structure.

Regarding the molecular weight of P(BSBPripol), it is possible to notice that the decrement was more remarkable, confirming the bulky nature of the degradation process. Comparing the films, the random copolymers degraded faster than the PBS samples and exhibited greater levels of variation in molecular weight. In particular, the P(BSBPripol) random copolymer sample was shown to be the fastest degrading sample, due to its low T_g, T_m and ΔH_m values. The slower degradation rate of random P(BSNS) copolymer can be correlated to its higher glass transition temperature, crystallinity degree and melting point. It should be recalled that the introduction of the NS subunit along the PBS main chain is responsible for a slight increase of chain rigidity (higher T_g), together with a decrease of both melting temperature and crystallinity (ΔH_m). On the contrary, the density of the -COOR- group remained

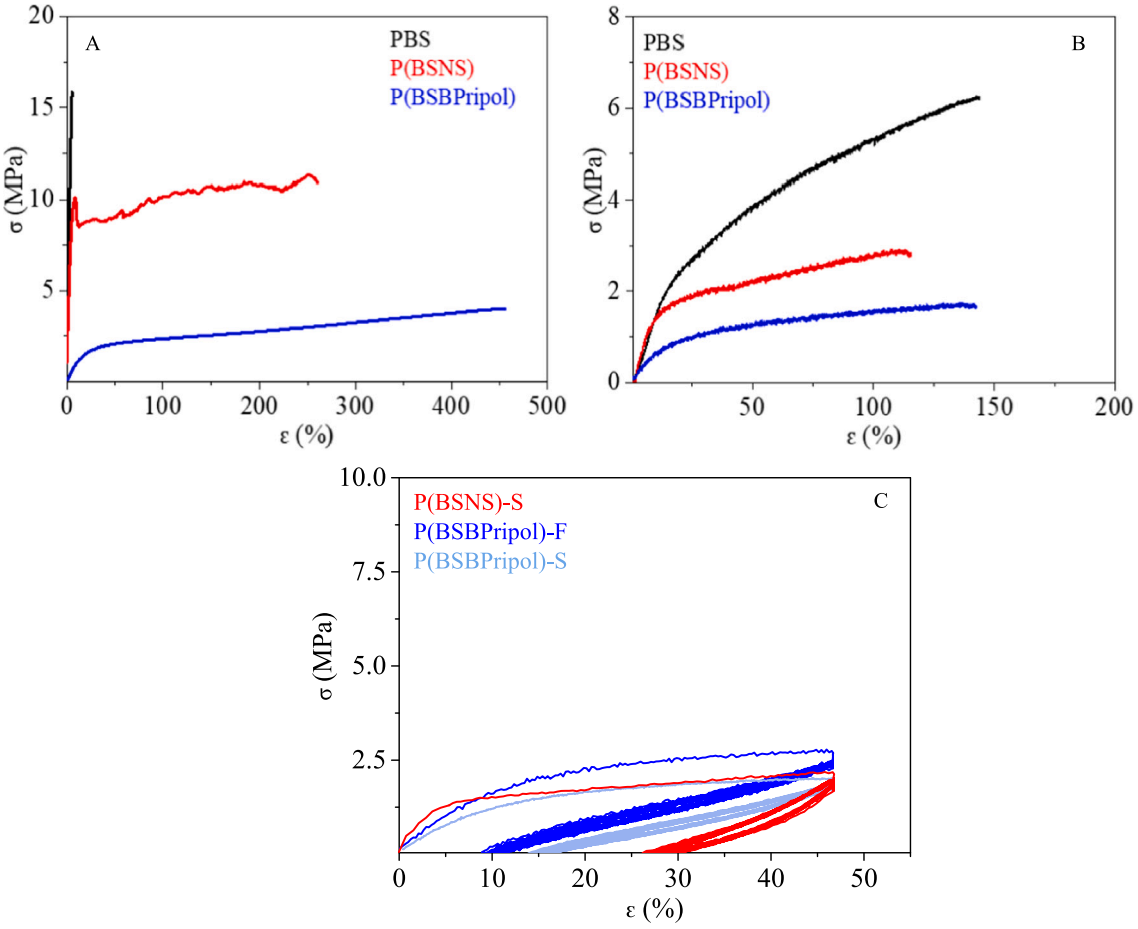

Fig. 3. Stress-strain curves of films (A) and scaffolds (B) of P(BSBPripol) and P(BSNS) compared to mechanical response of PBS; Cyclic loading curves of P(BSNS) scaffold and P(BSBPripol) in form of both film and scaffold (C).

Table 3
Thermal characterization and hydrolytic degradation data of PBS, P(BSBPripol) and P(BSNS) in form of films and scaffolds (*) after 15 weeks of incubation.

Polymer	T_g (°C)	T_m (°C)	ΔH_m (J/g)	WCA (°)	Weight loss (%)	Molecular weight loss (%)
PBS	−32	115	62	91 ± 2	2.0	35
P(BSNS)	−28	77	33	92 ± 3	3.0	42
P(BSBPripol)	−51	65	21	96 ± 2	2.0	47
PBS*	−32	114	64	101 ± 3	2.0 [16]	32 [16]
P(BSNS)*	−28	77	33	103 ± 2	4.8	45
P(BSBPripol)*	−51	64	23	109 ± 2	5.2	60

almost the same, with two glycolic subunits of very similar length (butylene vs. neopentyl glycol). In this view, the higher P(BSNS) weight loss with respect to PBS can be ascribed to the lower crystallinity degree.

For both copolymers, ^{1}H NMR analysis did not reveal any composition variation or the presence of any preferential attack of one of the two co-monomeric units present in the copolymers. Analogously, DSC and WAXS analyses did not show any difference in the crystallinity degree, suggesting that the degradation process involves both the crystalline and the amorphous phase.

As to the scaffolds, the trend is practically the same as that observed for films, even though occurring at faster rate due to the higher surface/volume ratio of the electrospun structure.

3.3. Biological evaluation of PBS-based scaffolds

In recent years, it has been demonstrated with strong evidence that the behaviour of human pluripotent stem cells is also intimately responsive to physical cell-ECM interactions, including sensitivity to stiffness and material topography [50–53]. Here, the hiPSCs line was cultured on P(BSNS) and P(BSBPripol) scaffolds to evaluate their ability to support stem cell proliferation, maintain stemness and support cardiac differentiation. hiPSCs represent a viable alternative cell source to human embryonic stem cells for regenerative purposes. It is important to note that PBS scaffold was not included in the following biological studies, as its characteristics were very similar to those of P(BSNS) random copolymer scaffolds.

3.3.1. hiPSCs stemness assessment onto scaffolds

Many studies have reported that substrate elasticity has an impact on the self-renewal and propagation of pluripotent stem cells [54–56]. Soft surfaces, particularly those that match the intrinsic stiffness of the inner cellular mass of ESCs (between 1 Pascal (Pa) and 1 kilopascal (kPa)), appear to be more effective than stiffer surfaces as they facilitate the generation of low cell-matrix traction [54]. P(BSNS) and P(BSBPripol) have a stiffness of approximately 24 megapascal (MPa) and 10 MPa, respectively, which suggested poor/altered interaction with hiPSCs.

Considering this, the fate of cells on P(BSNS) and P(BSBPripol) was studied by evaluating the viability and self-renewal characteristics on materials treated or not with a conventional coating, the Geltrex® (GTX). GTX is an extracellular matrix mimetic normally used to enhance the surface activity of scaffolds, with a similar composition to Matrigel and an average modulus of about 1 Pa [57–59]. Cells cultured on GTX-coated TCPS were used as a positive control. Initially, the average cell viability was assessed with the MTT assay at two-time frames (1 and 6 days) and expressed as a percentage of the GTX control (TCPS) (Fig. 4). For both marked control spots, viability was in the range of 91 %–98 %, with no statistically significant differences between GTX-coated P(BSNS) and P(BSBPripol) ($p > 0.05$). By contrast, significant reduction in cell viability was observed on the uncoated GTX scaffolds (approximately 80 and 60 % of reduction at 1 and 7 days of culture, respectively) than those GTX-coated, indicating initially incomplete hiPSCs adhesion to the uncoated-GTX substrates (Fig. 4).

Subsequently, the maintenance of the stemness phenotype of hiPSCs within the synthetic fibrous scaffolds (with/without GTX) for 6 days of culture was examined. RT-qPCR gene expression profiling revealed that in GTX-coated condition, hiPSCs cultured on P(BSNS) and P(BSBPripol) expressed similar levels of pluripotency genes OCT4, NANOG, SOX2, hTERT, KLF4 and cMYC compared to day 0 and on respect to TCPS conditions (Fig. 5a). These data were confirmed by immunofluorescence analysis: positive staining for both OCT4 and NANOG was observed in hiPSCs cultured on GTX-coated random-PBS scaffolds and, like the positive control, cell proliferation occurred in round, confluent colonies on each copolymer (Fig. 5b). In contrast, RT-qPCR data showed clear downregulation of all examined pluripotency genes in uncoated scaffolds compared to day 0 and on respect to TCPS with significant downregulation of OCT4, NANOG and cMYC (° and * $p < 0.05$ vs day 0 and TCPS, respectively). Afterwards, we compared the gene expression of hiPSCs cultured in uncoated GTX with those in GTX-coated materials: hiPSCs cultured on uncoated GTX showed lower expression of OCT4 (## $p < 0.01$), cMYC (# $p < 0.05$) and KLF4 (# $p < 0.05$), while no statistically significant difference was found between the two culture conditions (+/−GTX) on the expression of NANOG ($p > 0.05$), SOX2 ($p > 0.05$) and hTERT ($p > 0.05$). These data seem to indicate that the presence of a softer extracellular matrix coating created a better environment that facilitated the growth and maintenance of pluripotency on both types of materials, as it presumably masked, at least in the initial phase of the interaction, the stiffness of the underlying materials [36,60–64]. Furthermore, in both conditions with/without GTX, no significant differences were observed between P(BSNS) and P(BSBPripol) ($p > 0.05$), highlighting that a change in substrate's properties (chemical and stiffness) did not correspond to a change in the material's capability to influence the pluripotency characteristics.

3.3.2. Integrin and HYPPO pathway gene expression onto PBS-based scaffolds

The successful culture of hiPSCs on P(BSNS) and P(BSBPripol) surfaces has raised a fundamental question about the molecular mechanisms of cell attachment to these surfaces. Heterodimeric transmembrane integrin receptors are the main actors in bond formation between cell and extracellular matrix [65,66]. Integrin heterodimers (composed of the different β- and α-chains), which recognize and bind a specific ligand on the ECM, can help to regulate the different steps of the cell-ECM interaction by activating intracellular tyrosine kinase and phosphatase signaling to elicit downstream biochemical signals for pluripotency and stem cell differentiation [67–69]. Integrins are responsible for both ectodermal (α6, αv, β1, β3, β5), mesodermal (α5, α6, β1), and endodermal (α5, αv, β1, β3, β5) differentiation [70,71]. α1β1, α5β1 and α7β1 integrins are the most highly expressed integrin heterodimers in adult cardiomyocytes and the integrin α5 subunit is prevalent in fetal cardiomyocytes [72]. The composition and structure of the ECM substrate (including biomaterials) used for culture can influence the expression profile of integrins in human pluripotent stem cells. Here, gene expression analysis of some α and β integrins was performed in human iPSCs grown on each copolymer scaffold 6 days after seeding in both GTX-coated and uncoated surfaces (Fig. 6a and Fig. S4, respectively) [31,32]. As shown in Fig. 6a, at day 6 from cell seeding, there was significant upregulation of the α3, α5, α7, β1 genes in both GTX-coated copolymers and TCPS compared to day 0. In addition, the β5 gene was significantly downregulated at day 6 in both P(BSNS) and P(BSBPripol) as regards to day 0 and on respect to the positive control (*** $p < 0.001$ and °°° $p < 0.001$, respectively), while β3 was markedly upregulated in P(BSBPripol) as compared to day 0 (* $p < 0.05$) and P(BSNS), although not significantly in the latter case. With respect to cells cultured on TCPS, the expression of α7 (°°°° $p < 0.0001$) resulted increased only on P(BSNS). In contrast to what has been observed for pluripotency genes, material properties influenced the expression of integrin genes: a significant reduction of α5 (§§§§ $p < 0.0001$), α7 (§§§§ $p < 0.0001$), and β1 (§ $p < 0.05$) genes was measured on cells grown on P(BSBPripol) compared to P(BSNS). These data demonstrate how the cells perceive, despite the GTX coating, the physical properties of the underlying material, which thus appears to play a relevant role in determining the behaviour of the cells. Note that, in contrast to the GTX-coated condition, all the integrin genes analysed are increased on both the uncoated P(BSNS) and P(BSBPripol) compared to day 0, and some of them (α5, αV, α7 and β1) are more highly expressed than on TCPS (Fig. S4). The increased integrin expression may have been promoted by a close interaction of the cells with the surface topography, which, in contrast, could be inhibited/altered by GTX coating. Also, in uncoated culture conditions, differences were found between P(BSBPripol) and P(BSNS): a down-regulation of β1

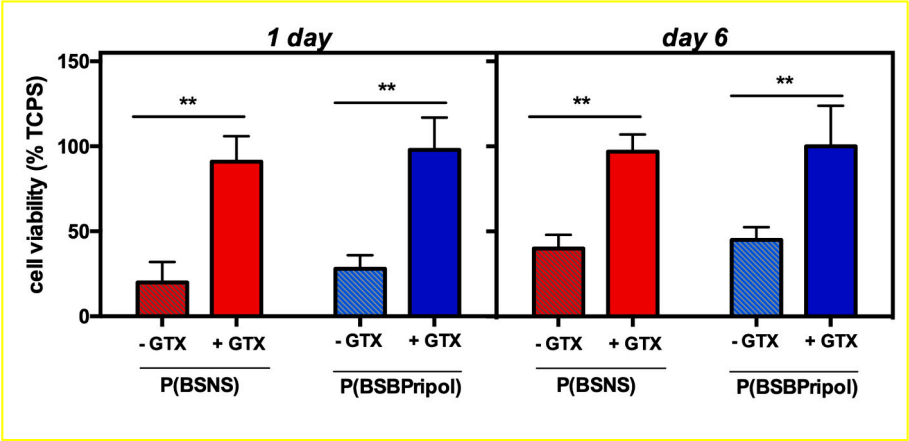

Fig. 4. Cell viability of hiPSCs cultured on P(BSNS) and P(BSBPripol), without GTX (−GTX) and with (+GTX) and coating for 1 and 6 days, respectively. Data are representative of ≥2 independent experiments and expressed as mean ± SD (**: $p < 0.01$). Cells cultured in GTX-coated TCPS were used as positive control.

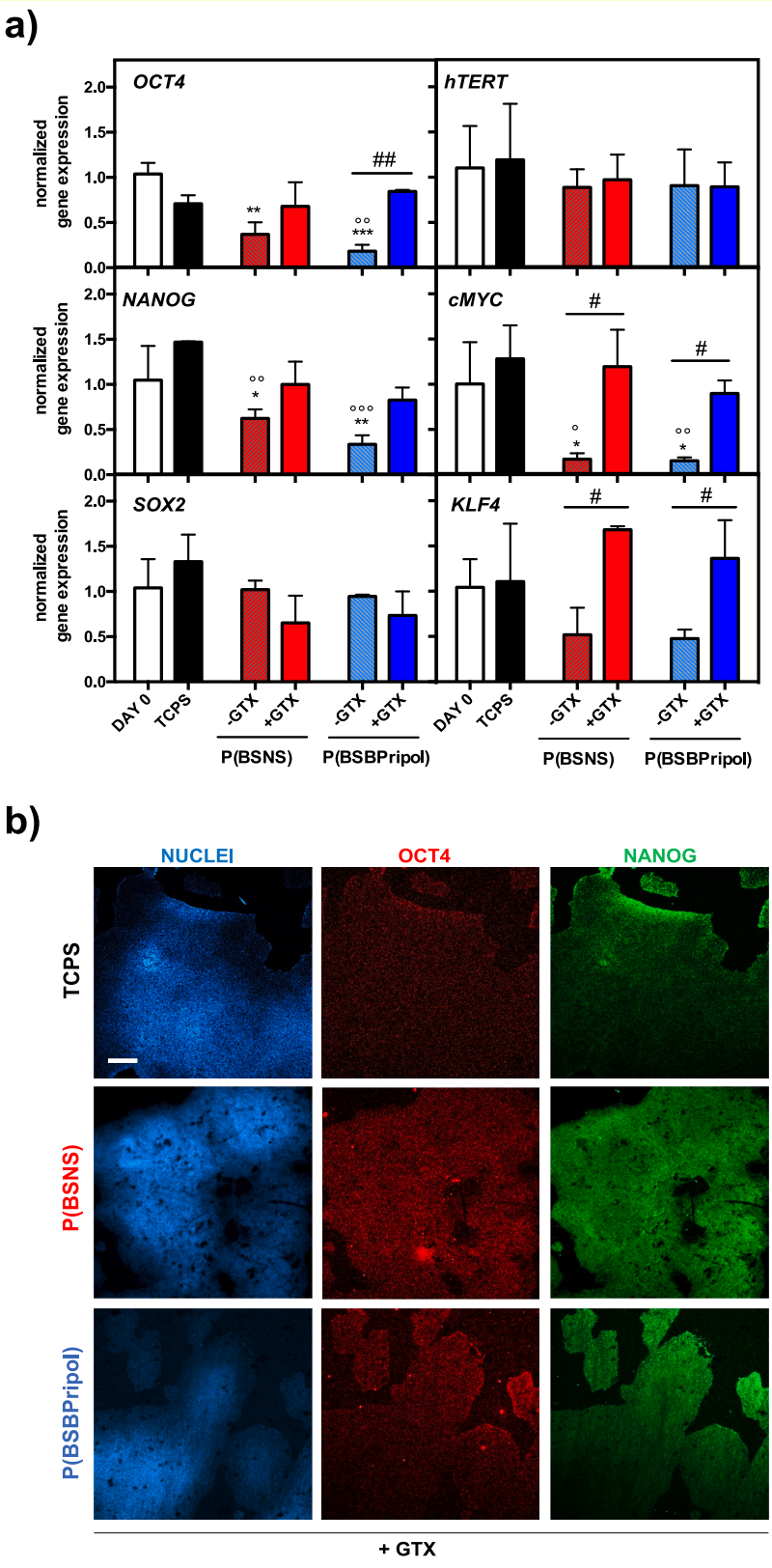

Fig. 5. Pluripotency markers in hiPCSs cultured for 6 days on P(BSNS) and P (BSBPripol), with/without GTX coating. a) RT-qPCR analysis for pluripotency markers on cells is shown. Expression of all genes was represented as a relative increase compared to the initial state (day 0). Data are representative of ≥2 independent experiments and expressed as mean ± SD. Symbols indicate statistical significance vs. day 0 (*), vs TCPS (°), vs - GTX (#) (* or ° or #: $p < 0.5$; ** or °° or ##: $p < 0.01$; *** or °°°: $p < 0.001$). b) Representative images of immunofluorescence on GTX-coated P(BSNS) and P(BSBPripol) staining to detect OCT4 (red, 633 Alexa Fluor) and NANOG (green, 488 Alexa Fluor); nuclei were counterstained with Hoechst 33342 (blue) (5× magnification and Scale bar = 200 μm. Cells cultured in GTX-coated TCPS were used as positive control for both a) and b) analyses. (For interpretation of the references to colour in this figure legend, the reader is referred to the web version of this article.)

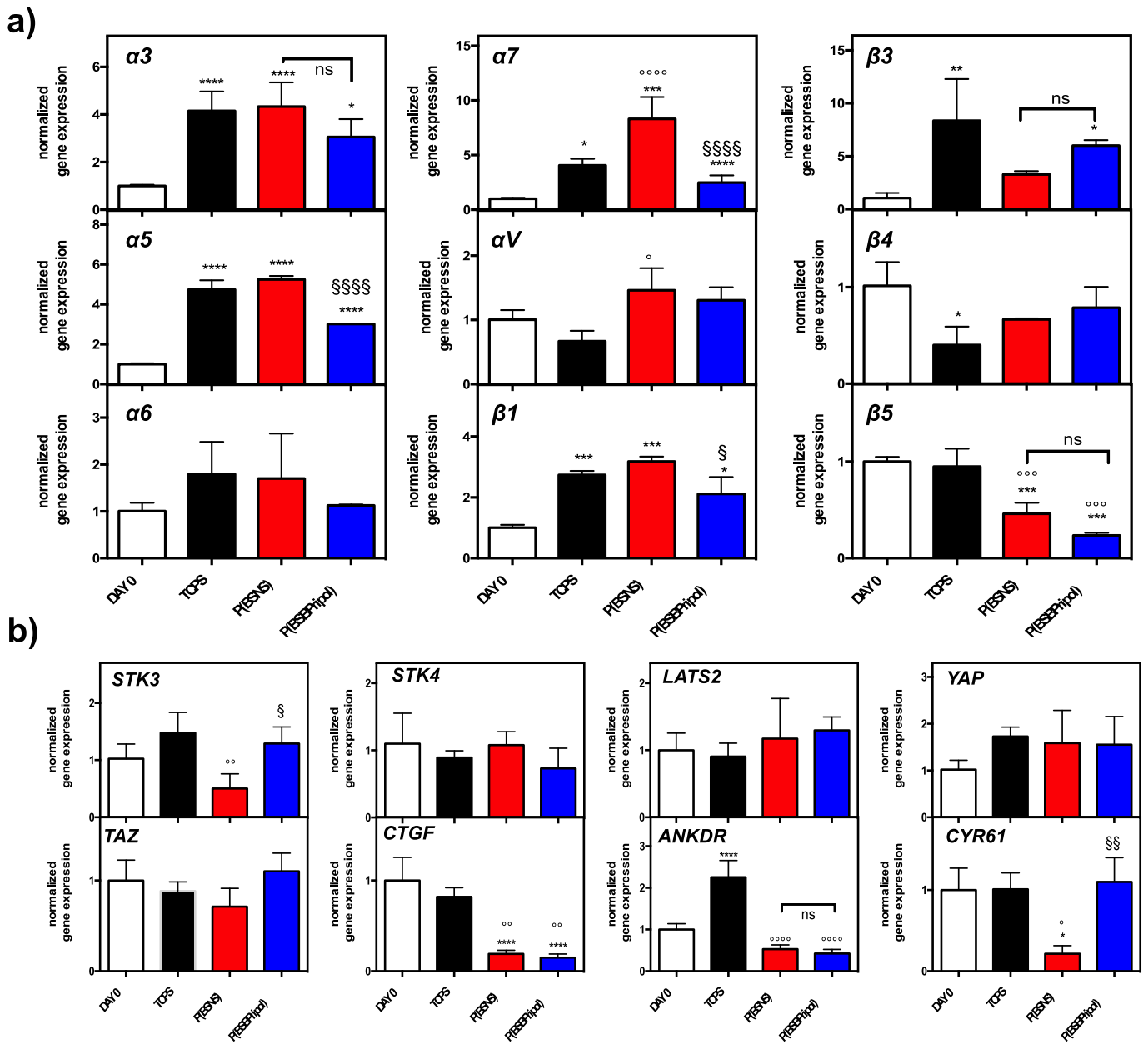

Fig. 6. Integrins and HYPPO pathway target gene expression. a) RT-qPCR analysis of indicated integrins subunits in hiPCSs cultured for 6 days on GTX-coated P(BSNS) and P(BSBPripol). Expression of all genes was represented as relative increase compared to the initial state (day 0). Cells cultured in GTX-coated TCPS were used as positive control. Data are representative of ≥2 independent experiments and expressed as mean ± SD). b) RT-qPCR analysis of HYPPO pathway genes in hiPCSs cultured for 6 days on GTX-coated P(BSNS) and P(BSBPripol). Expression of all genes was represented as a relative increase compared to the initial state (day 0). Cells cultured in GTX-coated TCPS were used as positive control. Data are representative of ≥2 independent experiments and expressed as mean ± SD). In a) and b) symbols indicate statistical significance vs. day 0 (*), vs TCPS (°), vs P(BSNS) (§), and ns = not significant (* or ° or §: $p < 0.5$; ** or °° or §§: $p < 0.01$; *** or °°° $p <$ 0.001; **** or °°°° or §§§§: $p < 0.0001$).

(§§§§ $p < 0.0001$) and β5 (§§§ $p < 0.001$) and as well as a significant upregulation of β3 in P(BSBPripol) (§ $p < 0.05$) (Fig. S4). Next, we investigated whether cells binding to the PBS-based copolymer scaffold could support and modulate the HIPPO pathway in hiPSCs (Fig. 6b). The HIPPO signaling cascade is an important pathway in adhesion-dependent stem cell proliferation, self-renewal, and differentiation [33,73,74]. The pathway is a kinase cascade involving mammalian STK3, STK4, LATS1 and LATS2. When activated, phosphorylation of STK3 and STK4 activates LATS1/2 kinases, which directly inactivate the Yes-associated protein (YAP) and the transcriptional coactivator with PDZ binding motif (TAZ), the two main functional outputs. The phosphorylated forms of YAP and TAZ are located in the cytoplasm, where they are degraded. In contrast, when no phosphorylated, YAP and TAZ migrate into the nucleus and regulate the expression of many target genes, including CTGF, ANKRD and CYR61. YAP and TAZ act as sensors and mediators of mechanical inputs from the extracellular matrix and their nuclear localization is drastically altered by matrix rigidity [75,76]. In particular, YAP/TAZ show a preferential cytoplasmic localization when cells can sense cell-to-cell contact, while moving into the nucleus when single cells are seeded on stiff substrates. Numerous studies have reported YAP/TAZ activation in diseased heart tissue, suggesting a potential role in heart repair and regeneration [77,78]. In addition, in vitro stimuli, including substrate rigidity and nanostructure topography trigger and control cardiomyocyte migration and

proliferation through YAP activation, although the underlying molecular mechanisms remain poorly characterized [79–81]. Regarding the pluripotency regulation, the exact role of YAP is unclear, complex and controversial and could be related to the versatile interaction of YAP with other intracellular components [78,82,83]. Different studies have proven that human ESCs also display great YAP/TAZ activity [78,84,85] and that its downregulation is correlated with differentiation in the neuroectoderm lineage [86]. However, there are several works showing that YAP/TAZ behaviour is related to the type of matrices in which the cells are cultured. However, even in this case, the data are sometimes conflicting: some works have demonstrated that on soft substrates hESCs express pluripotency markers, but the expression of YAP does not correlate directly with the pluripotency [55]; others showed that on rigid substrates YAP is active and localized in the nucleus, where it in turn enables the maintenance of self-renewal and stem cell proliferation [86]. In this study, we observed a drastic down-regulation of several YAP target genes in both GTX-coated (Fig. 6b) and uncoated (Fig. S5) scaffolds on respect to day 0 and compared to TCPS. The CTGF gene was significantly downregulated in cells cultured on both copolymer scaffolds under GTX (Fig. 6b) and uncoated conditions (Fig. S5), but no differences were observed between P(BSNS) and P(BSBPripol). Similarly, the level of ANKDR was reduced on respect to day 0 and if

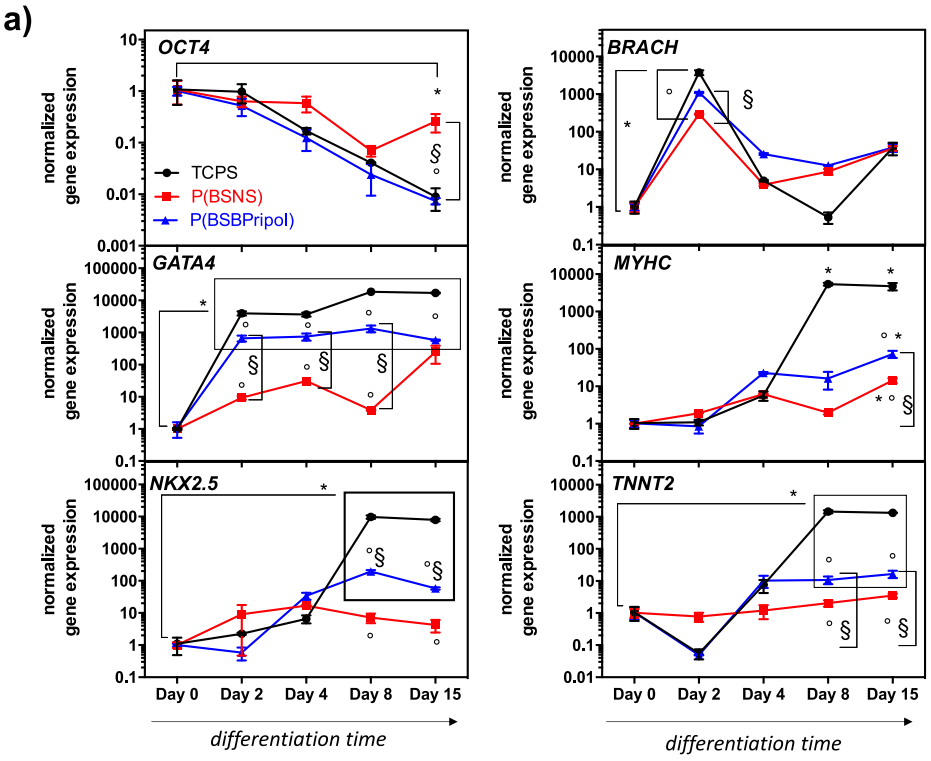

Fig. 7. Cardiac markers differentiation in hiPSCs-derived cardiomyocytes differentiated on GTX-coated P(BSNS) and P(BSBPripol). a) Time-course relative expression of genes involved in pluripotency (OCT4) and cardiac differentiation are shown. Expression of all genes was represented as relative increase compared to day 0 of differentiation. Data are representative of ≥2 independent experiments and expressed as mean ± SD (symbols indicate statistical significance vs. day 0 (* $p < 0.05$), vs TCPS (° $p < 0.05$), vs P(BSNS) (§ $p < 0.05$)). b) Representative images of immunofluorescence staining to detect the early cardiac progenitor marker NKX2.5 (red) and the later-stage cardiomyocyte marker ACTN2 (green); nuclei were counterstained with Hoechst 33342 (blue) (10× magnification and scale bar = 100 μm). Cells cultured in GFR-coated TCPS were used as positive control for both a) and b) analyses. (For interpretation of the references to colour in this figure legend, the reader is referred to the web version of this article.)

compared to TCPS, but again with no significant variation between the two copolymer scaffolds (Fig. 6b and S5). The notable difference between the random-PBS scaffolds was observed in the expression of CYR61, which was downregulated in P(BSNS) compared to P(BSBPripol) in the GTX condition (§§ $p < 0.01$, Fig. 6b) but not in the uncoated cultures (Fig. S5). CYR61 gene expression was significantly lower in P(BSNS) compared to day 0 and on respect to TCPS, both with GTX (* $p < 0.05$ and ° $p < 0.05$, respectively, Fig. 6b) and without GTX (** $p < 0.01$ and °° $p < 0.01$, respectively, Fig. S5). An interesting observation is that this finding was associated with lower expression of STK3, normally involved in the inactivation process of YAP, compared to day 0, on both TCPS and P(BSBPripol) in GTX cultures (Fig. 6b). In P(BSBPripol), the level of CYR61 was not altered in the GTX-coated material than at day 0 and in comparison to TCPS (Fig. 6b), whereas it was significantly decreased when the material was analysed without GTX (** $p < 0.01$ and °° $p < 0.01$ vs day 0 and TCPS, respectively, Fig. S5). Collectively these findings prove the involvement of HYPPO target genes as a transcriptional mediator (or mechano-sensors) for cellular responses to PBS-based copolymer scaffolds, although this engagement might play a different role (pro-pluripotency or pro-differentiation) depending on the presence or absence of GTX coating.

3.3.3. *hiPSCS cardiac differentiation assessment onto PBS-based scaffolds*

Subsequently, the time course of specific cardiac genes in human iPSCs differentiated into cardiomyocytes was studied (Fig. 7a). As expected, OCT4 gene expression decreased during differentiation and remained low on both substrates and control (day 0 vs day 15: * $p < 0.05$). Notably, the expression level of OCT4 was significantly higher for P(BSNS) than for P(BSBPripol) and TCPS at day 15 (§ $p < 0.05$). Compared to day 0, although there was upregulation of all cardiac differentiation genes examined over time, some differences were observed. BRACH, a gene of early mesoderm differentiation [87], was significantly increased at day 2 in TCPS, P(BSNS) and P(BSBPripol) compared to day 0 (* $p < 0.01$). Furthermore, at day 2, BRACH was significantly upregulated in P(BSBPripol) compared to P(BSNS) (§ $p < 0.05$). When compared to day 0, GATA4, an early cardiac differentiation gene [88], was significantly higher in both TCPS and P(BSBPripol) until the end of the differentiation time (* $p < 0.05$), whereas no significant increase was detected in P(BSNS). Remarkably, GATA4 expression was significantly increased in P(BSBPripol) compared to P(BSNS) (§ $p < 0.05$) as early as day 2 until day 8 of differentiation. Likewise, an overall increase in NKX2.5, another early cardiac differentiation gene [89], was observed in both TCPS and P(BSBPripol) compared to day 0 (* $p < 0.05$ at day 8 and day 15). The expression of this gene was found significantly lower in P(BSNS) than TCPS (° $p < 0.05$) and P(BSBPripol) (§ $p < 0.05$) at both day 8 and day 15, respectively. The expression level of MYHC and TNNT2, both involved in the later stages of cardiac differentiation [90], was shown to be also upregulated on both surfaces of the copolymer scaffold, as well as in TCPS in comparison to day 0. In detail, MYHC was found to be significantly higher in cells cultured on P(BSNS) and P(BSBPripol) at day 15 of differentiation than day 0 (* $p < 0.05$), but with a difference: the gene's expression resulted significantly higher on P(BSBPripol) compared to P(BSNS) (§ $p < 0.05$). Finally, significantly enhanced expression of TNNT2 was found on P(BSBPripol) at day 8 and 15 on respect to day 0 and if compared to P(BSNS) (* $p < 0.05$ and § $p < 0.05$). In general, these results show that the properties of the material profoundly influence the activation of cardiac genes. Indeed, cells cultured on P(BSBPripol), and not those on P(BSNS), exhibited increased expression of cardiac genes, although not at the same extent as cells cultured on TCPS (° $p < 0.05$). This was further confirmed by the immunostaining. Indeed, immunofluorescence analysis showed the presence of differentiated iPSC-CMs expressing the early cardiac progenitor marker NKX2.5 (red, within the nuclei) and the later-stage cardiomyocyte marker ACTN2 [91] (green, in the cytoplasm/cell membrane) on both copolymer scaffolds under investigation. However, the protein expression levels of ACTN2 in the scaffold-differentiated cells appeared to be less pronounced than in cells differentiated under control conditions (Fig. 7b), presumably, because it was harder to reach the later differentiation stages on the scaffolds under the conditions adopted.

3.3.4. *Integrin and HYPPO pathway gene expression in iPSCs-derived cardiomyocytes differentiated onto scaffolds*

Here, the gene expression analysis of some α and β integrins in cardiomyocytes derived from iPSCs differentiated on P(BSNS), P(BSBPripol) scaffolds and control (TCPS) was observed (Fig. 8). RT-qPCR data revealed a down-regulatory trend in the expression of α6, α7 and β5 subunit genes in both differentiated cells on P(BSNS) and P(BSBPripol) scaffolds compared to day 0 (* $p < 0.05$, Fig. 8a). Notably, the expression of α5 was more significantly induced in the P(BSBPripol) scaffolds compared to P(BSNS) (§ $p < 0.05$) and day 0 (* $p < 0.05$) samples during the differentiation period, suggesting that the former copolymer scaffold better supported cardiac differentiation (Fig. 8a). These data are in line with the expression of cardiac genes (Fig. 7a), which resulted more highly expressed on P(BSBPripol) rather than on P(BSNS). Furthermore, at day 4, the expression of integrin β3 was significantly increased compared to day 0 on the surface of P(BSBPripol) scaffold (* $p < 0.05$), even than on P(BSNS) (§ $p < 0.05$). Although the physiological relevance of the increase in integrin β3 in cardiomyocytes is unknown, we may hypothesize that focal contact through integrin β3 may facilitate cell adhesion and mediate the physical cues of the random-PBS scaffolds to modulate the function and differentiation of iPSCs. As stated previously, HYPPO signaling plays an important role during cardiac development [92]. We then assessed the gene expression of some HIPPO pathways components (Fig. 8b). Notably, along the cardiac differentiation time, like TCPS (day 15 vs day 0: * $p < 0.05$), a significant upregulation of YAP/TAZ expression was detected on P(BSBPripol) scaffold (day 15 vs day 0: * $p < 0.05$) but not on the P(BSNS) one. Of note, hiPSCs grown on P(BSNS) showed a lower LAT62 (at day 8), YAP (at day 8), TAZ (at day 8 and day 15) expression than on TCPS and P(BSBPripol) scaffold (° and § $p < 0.05$, respectively). As well as of YAP-target genes level (CTGF, ANKD3 and CYR61) was shown to be significantly higher on P(BSBPripol) scaffold with respect to day 0 (* $p < 0.05$) and CYR61 was noticeably greater from day 4 up to day 15 compared to TCPS (° $p < 0.05$). Compared to TCPS and P(BSBPripol), the expression of CTGF, ANKD3 and CYR61cells on P(BSNS) scaffold resulted significantly lower (° or § $p < 0.05$, respectively), once again highlighting how substrate nature can be crucial in activating specific biological responses. Since increased expression of cardiac genes was observed in particular on P(BSBPripol), we speculate that in differentiating cells the HYPPO signaling pathway may be engaged in cardiac differentiation of progenitor cells on this material by promoting the translocation of YAP/TAZ in the nucleus and thereby the expression of target genes.

4. Conclusions

Two new ad-hoc designed random PBS-based aliphatic copolyesters, one containing short ramifications (neopentyl glycol), the other long ramifications and PE-like segments (Pripol 1009), have been successfully synthesized to evaluate their possible use for the treatment of CVD, and in particular MI. As a known substrate, with appropriate mechanical properties (i.e., low rigidity, elasticity, and features similar to those of cells) ECM is necessary to ensure a healthy outcome. In this view, the chemical design, as well the processing was optimized to modulate the physicochemical properties of the starting homopolymer. Indeed, through copolymerization and even more by realization of fibrous scaffolds by electrospinning, it was possible to reduce PBS stiffness, the main limitation for applications in soft tissue engineering.

The introduction of Pripol 1009 moiety along PBS chain led to obtain a thermoplastic elastomeric scaffold with elastic modulus and elongation at break comparable to those of cardiac tissue. Conversely, the presence of neopentyl glycol moiety is responsible for a stiffer mechanical behaviour of the final material (P(BSNS)) with respect to P

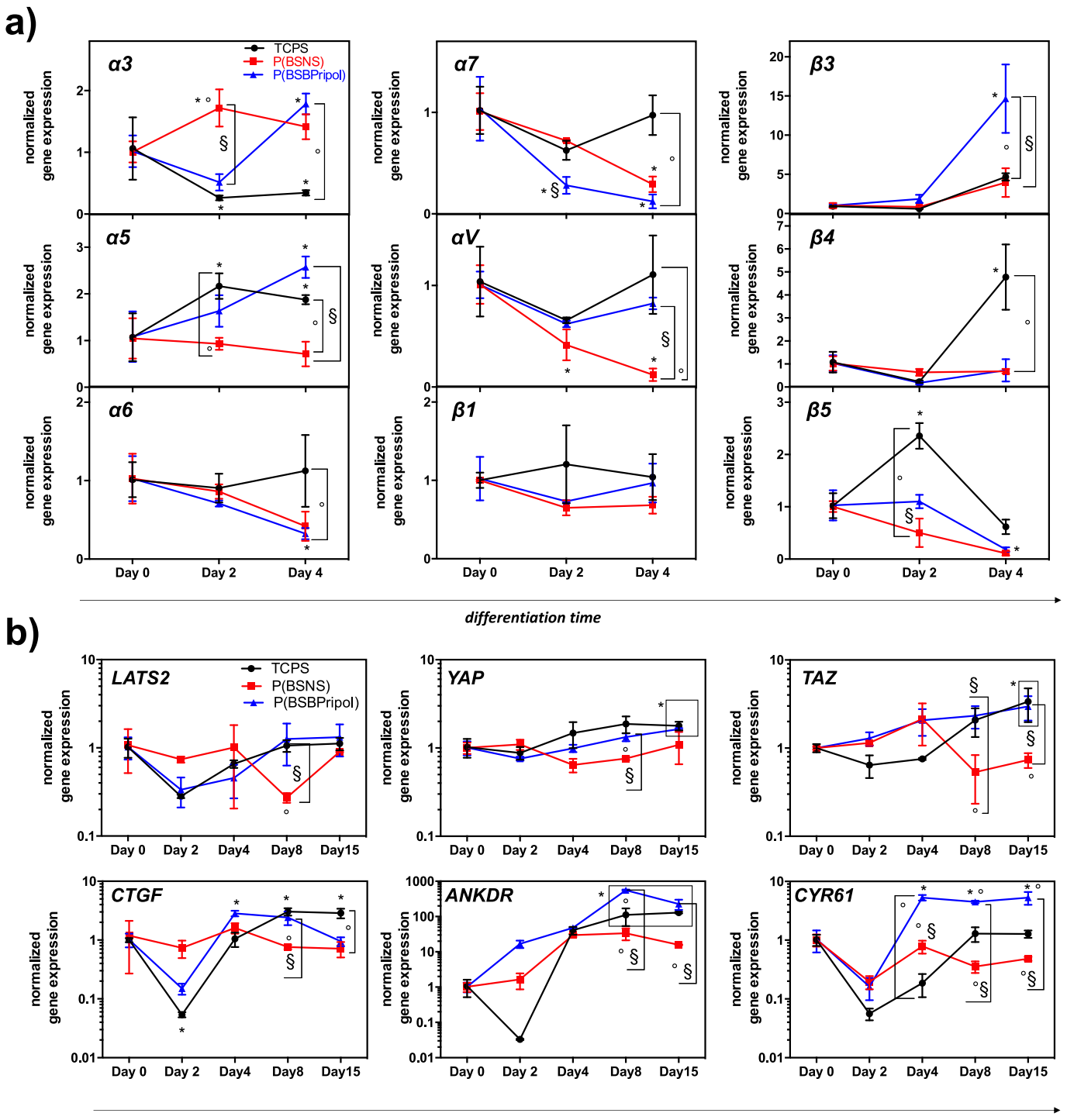

Fig. 8. RT-qPCR analysis of integrins subunits and HYPPO pathway genes in iPSCs-derived cardiomyocytes differentiated on GFR-coated P(BSNS) and P(BSBPripol). a) Time-course relative expression of indicated integrin genes is shown. Expression of all genes was represented as relative increase compared to day 0 of differentiation. Data are representative of ≥2 independent experiments and expressed as mean ± SD). b) Time-course relative expression of indicated genes is shown. Cells cultured in GTX-coated TCPS were used as positive control for both a) and b) analyses. Expression of all genes was represented as relative increase compared to day 0 of differentiation. Data are representative of ≥2 independent experiments and expressed as mean ± SD). Symbols in a) and b) indicate statistical significance vs. day 0 (* $p < 0.05$), vs TCPS (° $p < 0.05$), vs P(BSNS) (§ $p < 0.05$)).

(BSBPripol). This evidence was supported by DSC and WAXS results, which indicated that P(BSBPripol) is characterized by the lowest T_g and crystallinity degree, as a result of the plasticizing effect of the long aliphatic segments present in Pripol moiety. Conversely, in P(BSNS) copolymer, a reduction of crystallinity but also an increase of chain rigidity, i.e. an increase of T_g, was observed and is attributable to the steric hindrance effect of short side groups of neopentyl glycol.

Then, hiPSCs were cultured on both copolymeric scaffolds to evaluate their ability to support stem cell proliferation, maintain stemness and promote cardiac differentiation, knowing that the behaviour of cells is strictly related to physical cell-ECM interactions, as well as to substrate stiffness, topography, and chemical features. It should be emphasized that for the first time it was possible to successfully apply a cardiac differentiation protocol on hiPSCs cultivated on two non-

commercial synthetic copolyesters. The results are very interesting. First, on both copolymeric scaffolds a high cell viability of hiPSCs and a correct proliferation in round and confluent colonies was observed. However, the viability and maintenance of cell stemness on both scaffold surfaces were only achieved if a softer extracellular matrix coating (the GTX) was added to mask the rigid structure of both random-PBS materials. At the same time, it was observed that their different mechanical properties and the presence of the GTX coating profoundly influenced the gene expression of certain integrins and target genes of the HYPPO pathway. After the application of a proper differentiation protocol into cardiomyocytes, the P(BSBPripol) scaffold promoted a significant upregulation of cardiac markers involved in both early and mesoderm differentiation compared to P(BSNS) one, together with a simultaneously upregulation of α5 integrin and HYPPO pathway gene expression during the differentiation period. From a general perspective, these data would suggest that the signs raised from PBS-based scaffolds may influence the expression of cardiac genes in the progenitor cells with signals, arguably involving the activation of HYPPO pathways. In general, additional studies (such as phosphorylation of HYPPO kinases, quantification, and localization of YAP/TAZ) are paramount to verify the observations arising from this study and clarify exactly the biological response that is activated at the level of the two random-PBS materials here synthesized. In conclusion, we confirmed that the proper chemical design and, in turn, the matrix mechanical properties, play a key role both in supporting cell stemness, stem cell adhesion and proliferation, and in regulating cardiac progenitor behaviour and differentiation.

CRediT authorship contribution statement

The idea was developed by M.S. and N.L. Most experiments were performed by G.G., A.A. helped in the realization of scaffolds. M.G. performed the WAXS analysis. R.D. implemented the biocompatibility tests. G.G. assisted R.D. in doing experiments. R.D., N.B., M.S., N.L., L.V. and M.S. provided useful comments and contributed to methodology. The original draft was prepared by G.G. and N.B., and all the authors revised and reviewed the manuscript. All authors have given approval to the final version of the manuscript. We also thank Dr. Scott Burgess for English revision of the manuscript.

Declaration of competing interest

The authors declare that they have no known competing financial interests or personal relationships that could have appeared to influence the work reported in this paper.

Data availability

No data was used for the research described in the article.

Acknowledgments

Nora Bloise and Livia Visai acknowledge the grant of Ministry of University and Research (MUR) to the Department of Molecular Medicine (DMM) of the University of Pavia (NB and LV) under the initiative “Dipartimenti di Eccellenza (2018-2022) and (2023-2027)”. Maurilio Sampaolesi is supported by The Research Foundation Flanders (FWO) (#G066821N), INTERREG – Euregio Meuse-Rhine (GYM, Generate your muscle 2020-EMR116), and the Italian Ministry of Health, Ricerca Finalizzata (RF-2019-12369703).

Appendix A. Supplementary data

Supplementary data to this article can be found online at https://doi.org/10.1016/j.bioadv.2023.213583.

References

[1] A. Atala, Tissue engineering and regenerative medicine: concepts for clinical application, Rejuvenation Res 7 (1) (2004) 15–31, https://doi.org/10.1089/154916804323105053.
[2] B. Dhandayuthapani, Y. Yoshida, T. Maekawa, D.S. Kumar, Polymeric scaffolds in tissue engineering application: a review, International Journal of Polymer Science 2011 (2011), e290602, https://doi.org/10.1155/2011/290602.
[3] R.K. Kankala, K. Zhu, X.-N. Sun, C.-G. Liu, S.-B. Wang, A.-Z. Chen, Cardiac tissue engineering on the nanoscale, ACS Biomater Sci Eng 4 (3) (2018) 800–818, https://doi.org/10.1021/acsbiomaterials.7b00913.
[4] A. Mousavi, S. Vahdat, N. Baheiraei, M. Razavi, M.H. Norahan, H. Baharvand, Multifunctional conductive biomaterials as promising platforms for cardiac tissue engineering, ACS Biomater. Sci. Eng. 7 (1) (2021) 55–82, https://doi.org/10.1021/acsbiomaterials.0c01422.
[5] T. Ramos, L. Moroni, Tissue engineering and regenerative medicine 2019: the role of biofabrication—a year in review, Tissue Engineering Part C: Methods 26 (2) (2020) 91–106, https://doi.org/10.1089/ten.tec.2019.0344.
[6] M.E. Gomes, M.T. Rodrigues, R.M.A. Domingues, R.L. Reis, Tissue engineering and regenerative medicine: new trends and directions—a year in review, Tissue Engineering Part B: Reviews 23 (3) (2017) 211–224, https://doi.org/10.1089/ten.teb.2017.0081.
[7] L.A. Reis, L.L.Y. Chiu, N. Feric, L. Fu, M. Radisic, Biomaterials in myocardial tissue engineering, J Tissue Eng Regen Med 10 (1) (2016) 11–28, https://doi.org/10.1002/term.1944.
[8] D.E. Discher, P. Janmey, Y. Wang, Tissue cells feel and respond to the stiffness of their substrate, Science 310 (5751) (2005) 1139–1143, https://doi.org/10.1126/science.1116995.
[9] M. Massumi, M. Abasi, H. Babaloo, P. Terraf, M. Safi, M. Saeed, J. Barzin, M. Zandi, M. Soleimani, The effect of topography on differentiation fates of matrigel-coated mouse embryonic stem cells cultured on PLGA nanofibrous scaffolds, Tissue Eng Part A 18 (5–6) (2012) 609–620, https://doi.org/10.1089/ten.TEA.2011.0368.
[10] L. Mohammadi Amirabad, M. Massumi, M. Shamsara, I. Shabani, A. Amari, M. Mossahebi Mohammadi, S. Hosseinzadeh, S. Vakilian, S.K. Steinbach, M. R. Khorramizadeh, M. Soleimani, J. Barzin, Enhanced cardiac differentiation of human cardiovascular disease patient-specific induced pluripotent stem cells by applying unidirectional electrical pulses using aligned electroactive nanofibrous scaffolds, ACS Appl. Mater. Interfaces 9 (8) (2017) 6849–6864, https://doi.org/10.1021/acsami.6b15271.
[11] A. Higuchi, Q.-D. Ling, Y.-A. Ko, Y. Chang, A. Umezawa, Biomaterials for the feeder-free culture of human embryonic stem cells and induced pluripotent stem cells, Chem. Rev. 111 (5) (2011) 3021–3035, https://doi.org/10.1021/cr1003612.
[12] I. Manavitehrani, A. Fathi, H. Badr, S. Daly, A. Negahi Shirazi, F. Dehghani, Biomedical applications of biodegradable polyesters, Polymers (Basel) 8 (1) (2016) 20, https://doi.org/10.3390/polym8010020.
[13] M. Gigli, M. Fabbri, N. Lotti, R. Gamberini, B. Rimini, A. Munari, Poly(butylene succinate)-based polyesters for biomedical applications: a review, European Polymer Journal 75 (2016) 431–460, https://doi.org/10.1016/j.eurpolymj.2016.01.016.
[14] C. Gualandi, M. Soccio, E. Saino, M.L. Focarete, N. Lotti, A. Munari, L. Moroni, L. Visai, Easily synthesized novel biodegradable copolyesters with adjustable properties for biomedical applications, Soft Matter 8 (20) (2012) 5466–5476, https://doi.org/10.1039/C2SM25308A.
[15] M. Gigli, N. Lotti, M. Gazzano, L. Finelli, A. Munari, Synthesis and characterization of novel poly(butylene succinate)-based copolyesters designed as potential candidates for soft tissue engineering, Polymer Engineering & Science 53 (3) (2013) 491–501, https://doi.org/10.1002/pen.23289.
[16] C. Gualandi, M. Soccio, M. Govoni, S. Valente, N. Lotti, A. Munari, E. Giordano, G. Pasquinelli, M.L. Focarete, Poly(butylene/diethylene glycol succinate) multiblock copolyester as a candidate biomaterial for soft tissue engineering: solid-state properties, degradability, and biocompatibility, Journal of Bioactive and Compatible Polymers 27 (3) (2012) 244–264, https://doi.org/10.1177/0883911512440536.
[17] G. Guidotti, M. Soccio, M. Gazzano, L. Fusaro, F. Boccafoschi, A. Munari, N. Lotti, New thermoplastic elastomer triblock copolymer of PLLA for cardiovascular tissue engineering: annealing as efficient tool to tailor the solid-state properties, Polymer 213 (123) (2021) 336, https://doi.org/10.1016/j.polymer.2020.123336.
[18] G. Guidotti, M. Soccio, M. Gazzano, N. Bloise, G. Bruni, A. Aluigi, L. Visai, A. Munari, N. Lotti, Biocompatible PBS-based copolymer for soft tissue engineering: introduction of disulfide bonds as winning tool to tune the final properties, Polymer Degradation and Stability 182 (109) (2020) 403, https://doi.org/10.1016/j.polymdegradstab. 2020.109403.
[19] G. Guidotti, M. Soccio, T. Posati, G. Sotgiu, M. Tiboni, M. Barbalinardo, F. Valle, L. Casettari, R. Zamboni, N. Lotti, A. Aluigi, Regenerated wool keratin-polybutylene succinate nanofibrous mats for drug delivery and cells culture, Polymer Degradation and Stability 179 (109) (2020) 272, https://doi.org/10.1016/j.polymdegradstab. 2020.109272.
[20] M. Fabbri, G. Guidotti, M. Soccio, N. Lotti, M. Govoni, E. Giordano, M. Gazzano, R. Gamberini, B. Rimini, A. Munari, Novel biocompatible pbs-based random copolymers containing PEG-like sequences for biomedical applications: from drug delivery to tissue engineering, Polymer Degradation and Stability 153 (2018) 53–62, https://doi.org/10.1016/j.polymdegradstab. 2018.04.011.
[21] J. Domínguez-Robles, E. Larrañeta, M.L. Fong, N.K. Martin, N.J. Irwin, P. Mutjé, Q. Tarrés, M. Delgado-Aguilar, Lignin/poly(butylene succinate) composites with antioxidant and antibacterial properties for potential biomedical applications,

International Journal of Biological Macromolecules 145 (2020) 92–99, https://doi.org/10.1016/j.ijbiomac.2019.12.146.
[22] J. Zhou, X. Wang, K. Hua, C. Duan, W. Zhang, J. Ji, X. Yang, Enhanced mechanical properties and degradability of poly(butylene succinate) and poly(lactic acid) blends, Iran Polym J 22 (4) (2013) 267–275, https://doi.org/10.1007/s13726-013-0124-8.
[23] M. Tallawi, D.C. Zebrowski, R. Rai, J.A. Roether, D.W. Schubert, M. El Fray, F. B. Engel, K.E. Aifantis, A.R. Boccaccini, Poly(glycerol sebacate)/poly(butylene succinate-butylene dilinoleate) fibrous scaffolds for cardiac tissue engineering, Tissue Engineering Part C: Methods 21 (6) (2015) 585–596, https://doi.org/10.1089/ten.tec.2014.0445.
[24] L. Liverani, A. Piegat, A. Niemczyk, M. El Fray, A.R. Boccaccini, Electrospun fibres of poly(butylene succinate–co–dilinoleic succinate) and its blend with poly (glycerol sebacate) for soft tissue engineering applications, European Polymer Journal 81 (2016) 295–306, https://doi.org/10.1016/j.eurpolymj.2016.06.009.
[25] J.T. Oliveira, V.M. Correlo, P.C. Sol, A.R. Costa-Pinto, P.B. Malafaya, A.J. Salgado, M. Bhattacharya, P. Charbord, N.M. Neves, R.L. Reis, Assessment of the suitability of chitosan/polybutylene succinate scaffolds seeded with mouse mesenchymal progenitor cells for a cartilage tissue engineering approach, Tissue Engineering Part A 14 (10) (2008) 1651–1661, https://doi.org/10.1089/ten.tea.2007.0307.
[26] E. Poon, C. Kong, R.A. Li, Human pluripotent stem cell-based approaches for myocardial repair: from the electrophysiological perspective, Mol. Pharmaceutics 8 (5) (2011) 1495–1504, https://doi.org/10.1021/mp2002363.
[27] E. Kingham, R.O.C. Oreffo, Embryonic and induced pluripotent stem cells: understanding, creating, and exploiting the nano-niche for regenerative medicine, ACS Nano 7 (3) (2013) 1867–1881, https://doi.org/10.1021/nn3037094.
[28] V. Buchholz, S. Agarwal, A. Greiner, Synthesis and enzymatic degradation of soft aliphatic polyesters, Macromolecular Bioscience 16 (2) (2016) 207–213, https://doi.org/10.1002/mabi.201500279.
[29] D.P.R. Kint, A. Martínez de Ilarduya, A. Sansalvadó, J. Ferrer, J.I. Iribarren, S. Muñoz-Guerra, Structural characterization and thermal properties of poly (ethylene terephthalate) copolymers containing 2-butyl-2-ethyl-1,3-propanediol, Journal of Applied Polymer Science 86 (5) (2002) 1077–1086, https://doi.org/10.1002/app.11057.
[30] S. Quattrosoldi, M. Soccio, M. Gazzano, N. Lotti, A. Munari, Fully biobased, elastomeric and compostable random copolyesters of poly(butylene succinate) containing pripol 1009 moieties: structure-property relationship, Polymer Degradation and Stability 178 (109) (2020) 189, https://doi.org/10.1016/j.polymdegradstab. 2020.109189.
[31] T.J. Rowland, L.M. Miller, A.J. Blaschke, E.L. Doss, A.J. Bonham, S.T. Hikita, L. V. Johnson, D.O. Clegg, Roles of integrins in human induced pluripotent stem cell growth on matrigel and vitronectin, Stem Cells and Development 19 (8) (2010) 1231–1240, https://doi.org/10.1089/scd.2009.0328.
[32] Y. Hayashi, M.K. Furue, Biological effects of culture substrates on human pluripotent stem cells, Stem Cells International 2016 (2016), e5380560, https://doi.org/10.1155/2016/5380560.
[33] X. Cao, C. Wang, J. Liu, B. Zhao, Regulation and functions of the hippo pathway in stemness and differentiation, Acta Biochim Biophys Sin (Shanghai) 52 (7) (2020) 736–748, https://doi.org/10.1093/abbs/gmaa048.
[34] H. Liu, D. Jiang, F. Chi, B. Zhao, The hippo pathway regulates stem cell proliferation, self-renewal, and differentiation, Protein Cell 3 (4) (2012) 291–304, https://doi.org/10.1007/s13238-012-2919-3.
[35] G. Guidotti, M. Soccio, V. Siracusa, M. Gazzano, E. Salatelli, A. Munari, N. Lotti, Novel random PBS-based copolymers containing aliphatic side chains for sustainable flexible food packaging, Polymers (Basel) 9 (12) (2017) 724, https://doi.org/10.3390/polym9120724.
[36] C. Gualandi, N. Bloise, N. Mauro, P. Ferruti, A. Manfredi, M. Sampaolesi, A. Liguori, R. Laurita, M. Gherardi, V. Colombo, L. Visai, M.L. Focarete, E. Ranucci, Poly-l-lactic acid nanofiber–polyamidoamine hydrogel composites: preparation, properties, and preliminary evaluation as scaffolds for human pluripotent stem cell culturing, Macromolecular Bioscience 16 (10) (2016) 1533–1544, https://doi.org/10.1002/mabi.201600061.
[37] M. Soccio, N. Lotti, L. Finelli, M. Gazzano, A. Munari, Neopenthyl glycol containing poly(propylene azelate)s: synthesis and thermal properties, European Polymer Journal 43 (8) (2007) 3301–3313, https://doi.org/10.1016/j.eurpolymj.2007.06.011.
[38] M. Soccio, N. Lotti, L. Finelli, M. Gazzano, A. Munari, Neopenthyl glycol containing poly(propylene terephthalate)s: structure–properties relationships, Journal of Polymer Science Part B: Polymer Physics 46 (2) (2008) 170–181, https://doi.org/10.1002/polb.21352.
[39] Y. Zheng, P. Pan, Crystallization of biodegradable and biobased polyesters: polymorphism, cocrystallization, and structure-property relationship, Progress in Polymer Science 109 (101) (2020) 291, https://doi.org/10.1016/j.progpolymsci.2020.101291.
[40] P. Pan, Y. Inoue, Polymorphism and isomorphism in biodegradable polyesters, Prog Polym Sci 34 (2009) 605–640, https://doi.org/10.1016/j.progpolymsci.2009.01.003.
[41] A. Larrañaga, E. Lizundia, A Review on the thermomechanical properties and biodegradation behaviour of polyesters, European Polymer Journal 121 (109) (2019) 296, https://doi.org/10.1016/j.eurpolymj.2019.109296.
[42] Y. Ichikawa, H. Kondo, Y. Igarashi, K. Noguchi, K. Okuyama, J. Washiyama, Crystal structures of α and β forms of poly(tetramethylene succinate), Polymer 41 (12) (2000) 4719–4727, https://doi.org/10.1016/S0032-3861(99)00659-X.
[43] M.C. Righetti, M.L. Di Lorenzo, D. Cavallo, A.J. Müller, M. Gazzano, Structural evolution of poly(butylene succinate) crystals on heating with the formation of a dual lamellar population, as monitored by temperature-dependent WAXS/SAXS analysis, Polymer 268 (125) (2023) 711, https://doi.org/10.1016/j.polymer.2023.125711.
[44] Q.-Z. Chen, A. Bismarck, U. Hansen, S. Junaid, M.Q. Tran, S.E. Harding, N.N. Ali, A.R. Boccaccini, Characterization of a soft elastomer poly(glycerol sebacate) designed to match the mechanical properties of myocardial tissue, Biomaterials 29 (1) (2008) 47–57, https://doi.org/10.1016/j.biomaterials.2007.09.010.
[45] D. Kai, M.P. Prabhakaran, G. Jin, S. Ramakrishna, Polypyrrole-contained electrospun conductive nanofibrous membranes for cardiac tissue engineering, Journal of Biomedical Materials Research Part A 99A (3) (2011) 376–385, https://doi.org/10.1002/jbm.a.33200.
[46] Y. Liu, S. Wang, R. Zhang, Composite poly(lactic acid)/chitosan nanofibrous scaffolds for cardiac tissue engineering, Int J Biol Macromol 103 (2017) 1130–1137, https://doi.org/10.1016/j.ijbiomac.2017.05.101.
[47] A.P. Pêgo, A.A. Poot, D.W. Grijpma, J. Feijen, Biodegradable elastomeric scaffolds for soft tissue engineering, Journal of Controlled Release 87 (1) (2003) 69–79, https://doi.org/10.1016/S0168-3659(02)00351-6.
[48] Q.-Z. Chen, S.E. Harding, N.N. Ali, A.R. Lyon, A.R. Boccaccini, Biomaterials in cardiac tissue engineering: ten years of research survey, Materials Science and Engineering: R: Reports 59 (1) (2008) 1–37, https://doi.org/10.1016/j.mser.2007.08.001.
[49] M. Soccio, N. Lotti, M. Gazzano, M. Govoni, E. Giordano, A. Munari, Molecular architecture and solid-state properties of novel biocompatible PBS-based copolyesters containing sulphur atoms, Reactive and Functional Polymers 72 (11) (2012) 856–867, https://doi.org/10.1016/j.reactfunctpolym.2012.08.002.
[50] W.L. Murphy, T.C. McDevitt, A.J. Engler, Materials as stem cell regulators, Nature Mater 13 (6) (2014) 547–557, https://doi.org/10.1038/nmat3937.
[51] T. Perestrelo, M. Correia, J. Ramalho-Santos, D. Wirtz, Metabolic and mechanical cues regulating pluripotent stem cell fate, Trends Cell Biol 28 (12) (2018) 1014–1029, https://doi.org/10.1016/j.tcb.2018.09.005.
[52] K.A. Gultian, R. Gandhi, K. Sarin, M. Sladkova-Faure, M. Zimmer, G.M. de Peppo, S.L. Vega, Human induced mesenchymal stem cells display increased sensitivity to matrix stiffness, Sci Rep 12 (1) (2022) 8483, https://doi.org/10.1038/s41598-022-12,143-2.
[53] A.M. Bosworth, H. Kim, K.P. O'Grady, I. Richter, L. Lee, B.J. O'Grady, E. S. Lippmann, Influence of substrate stiffness on barrier function in an ipsc-derived in vitro blood-brain barrier model, Cell Mol Bioeng 15 (1) (2022) 31–42, https://doi.org/10.1007/s12195-021-00706-8.
[54] F. Chowdhury, Y. Li, Y.-C. Poh, T. Yokohama-Tamaki, N. Wang, T.S. Tanaka, Soft substrates promote homogeneous self-renewal of embryonic stem cells via downregulating cell-matrix tractions, PLoS One 5 (12) (2010), e15655, https://doi.org/10.1371/journal.pone.0015655.
[55] J.K. Virdi, P. Pethe, Soft substrate maintains stemness and pluripotent stem cell-like phenotype of human embryonic stem cells under defined culture conditions, Cytotechnology 74 (4) (2022) 479–489, https://doi.org/10.1007/s10616-022-00537-z.
[56] H. Gerardo, A. Lima, J. Carvalho, J.R.D. Ramos, S. Couceiro, R.D.M. Travasso, R. Pires das Neves, M. Grãos, Soft culture substrates favor stem-like cellular phenotype and facilitate reprogramming of human mesenchymal stem/stromal cells (HMSCs) through mechanotransduction, Sci Rep 9 (1) (2019) 9086, https://doi.org/10.1038/s41598-019-45,352-3.
[57] C. Kothapalli, G. Mahajan, K. Farrell, Substrate stiffness induced mechanotransduction regulates temporal evolution of human fetal neural progenitor cell phenotype, differentiation, and biomechanics, Biomater. Sci. 8 (19) (2020) 5452–5464, https://doi.org/10.1039/D0BM01349H.
[58] S.H. Maxian, T. Di Stefano, M.C. Melican, M.L. Tiku, J.P. Zawadsky, Bone cell behaviour on matrigel®-coated Ca/P coatings of varying crystallinities, Journal of Biomedical Materials Research 40 (2) (1998) 171–179, https://doi.org/10.1002/(SICI)1097-4636(199805)40:2 < 171::AID-JBM1 > 3.0.CO;2-I.
[59] M. Schubert, B. Binnewerg, A. Voronkina, L. Muzychka, M. Wysokowski, I. Petrenko, V. Kovalchuk, M. Tsurkan, R. Martinovic, N. Bechmann, V. N. Ivanenko, A. Fursov, O.B. Smolii, J. Fromont, Y. Joseph, S.R. Bornstein, M. Giovine, D. Erpenbeck, K. Guan, H. Ehrlich, Naturally prefabricated marine biomaterials: isolation and applications of flat chitinous 3D scaffolds from ianthella labyrinthus (demospongiae: verongiida), Int J Mol Sci 20 (20) (2019) 5105, https://doi.org/10.3390/ijms20205105.
[60] J.W. Lambshead, L. Meagher, C. O'Brien, A.L. Laslett, Defining synthetic surfaces for human pluripotent stem cell culture, Cell Regen 2 (1) (2013) 7, https://doi.org/10.1186/2045-9769-2-7.
[61] C. Mancino, T. Hendrickson, L.V. Whitney, F. Paradiso, S. Abasi, E. Tasciotti, F. Taraballi, A. Guiseppi-Elie, Electrospun electroconductive constructs of aligned fibres for cardiac tissue engineering, Nanomedicine 44 (102) (2022) 567, https://doi.org/10.1016/j.nano.2022.102567.
[62] P. Zhou, L. Qin, Z. Ge, B. Xie, H. Huang, F. He, S. Ma, L. Ren, J. Shi, S. Pei, G. Dong, Y. Qi, F. Lan, Design of chemically defined synthetic substrate surfaces for the in vitro maintenance of human pluripotent stem cells: a review, J Biomed Mater Res B Appl Biomater 110 (8) (2022) 1968–1990, https://doi.org/10.1002/jbm.b.35034.
[63] T. Richardson, C. Wiegand, F. Adisa, K. Ravikumar, J. Candiello, P. Kumta, I. Banerjee, Engineered peptide modified hydrogel platform for propagation of human pluripotent stem cells, Acta Biomaterialia 113 (2020) 228–239, https://doi.org/10.1016/j.actbio.2020.06.034.
[64] P. Zhou, F. Wu, T. Zhou, X. Cai, S. Zhang, X. Zhang, Q. Li, Y. Li, Y. Zheng, M. Wang, F. Lan, G. Pan, D. Pei, S. Wei, Simple and versatile synthetic polydopamine-based surface supports reprogramming of human somatic cells and long-term self-renewal of human pluripotent stem cells under defined conditions, Biomaterials 87 (2016) 1–17, https://doi.org/10.1016/j.biomaterials.2016.02.012.

[65] J. Du, X. Chen, X. Liang, G. Zhang, J. Xu, L. He, Q. Zhan, X.-Q. Feng, S. Chien, C. Yang, Integrin activation and internalization on soft ECM as a mechanism of induction of stem cell differentiation by ECM elasticity, Proc Natl Acad Sci U S A 108 (23) (2011) 9466–9471, https://doi.org/10.1073/pnas.1106467108.
[66] J. Luo, M. Walker, Y. Xiao, H. Donnelly, M.J. Dalby, M. Salmeron-Sanchez, The influence of nanotopography on cell behaviour through interactions with the extracellular matrix - a review, Bioact Mater 15 (2022) 145–159, https://doi.org/10.1016/j.bioactmat.2021.11.024.
[67] L. Vitillo, S.J. Kimber, Integrin and FAK regulation of human pluripotent stem cells, Curr Stem Cell Rep 3 (4) (2017) 358–365, https://doi.org/10.1007/s40778-017-0100-x.
[68] S. Taleahmad, M. Mirzaei, A. Samadian, S.-N. Hassani, P.A. Haynes, G.H. Salekdeh, H. Baharvand, Low focal adhesion signaling promotes ground state pluripotency of mouse embryonic stem cells, J. Proteome Res. 16 (10) (2017) 3585–3595, https://doi.org/10.1021/acs.jproteome.7b00322.
[69] L.G. Villa-Diaz, J.K. Kim, A. Laperle, S.P. Palecek, P.H. Krebsbach, Inhibition of focal adhesion kinase signaling by integrin α6β1 supports human pluripotent stem cell self-renewal, STEM CELLS 34 (7) (2016) 1753–1764, https://doi.org/10.1002/stem.2349.
[70] H. Wang, X. Luo, J. Leighton, Extracellular matrix and integrins in embryonic stem cell differentiation, Biochem Insights 8 (Suppl. 2) (2015) 15–21, https://doi.org/10.4137/BCI.S30377.
[71] R. Thomas, V. Menon, R. Mani, J. Pruszak, Glycan epitope and integrin expression dynamics characterize neural crest epithelial-to-mesenchymal transition (EMT) in human pluripotent stem cell differentiation, Stem Cell Rev Rep 18 (8) (2022) 2952–2965, https://doi.org/10.1007/s12015-022-10,393-1.
[72] G. Neiman, M.A. Scarafía, A. La Greca, N.L. Santín Velazque, X. Garate, A. Waisman, A.M. Möbbs, T.H. Kasai-Brunswick, F. Mesquita, D. Martire-Greco, L. N. Moro, C. Luzzani, A. Bastos Carvalho, G.E. Sevlever, A. Campos de Carvalho, A. S. Guberman, S.G. Miriuka, Integrin alpha-5 subunit is critical for the early stages of human pluripotent stem cell cardiac differentiation, Scientific Reports 9 (1) (2019) 18,077, https://doi.org/10.1038/s41598-019-54,352-2.
[73] F. Passaro, I. De Martino, F. Zambelli, G. Di Benedetto, M. Barbato, A.M. D'Erchia, C. Manzari, G. Pesole, M. Mutarelli, D. Cacchiarelli, D. Antonini, S. Parisi, T. Russo, YAP contributes to DNA methylation remodeling upon mouse embryonic stem cell differentiation, J Biol Chem 296 (100) (2021) 138, https://doi.org/10.1074/jbc.RA120.015896.
[74] N.D. Zeybek, E. Baysal, O. Bozdemir, E. Buber, Hippo signaling: a stress response pathway in stem cells, Curr Stem Cell Res Ther 16 (7) (2021) 824–839, https://doi.org/10.2174/1574888X16666210712100002.
[75] S. Dupont, L. Morsut, M. Aragona, E. Enzo, S. Giulitti, M. Cordenonsi, F. Zanconato, J. Le Digabel, M. Forcato, S. Bicciato, N. Elvassore, S. Piccolo, Role of YAP/TAZ in mechanotransduction, Nature 474 (7350) (2011) 179–183, https://doi.org/10.1038/nature10137.
[76] D. Ngai, A.L. Mohabeer, A. Mao, M. Lino, M.P. Bendeck, Stiffness-responsive feedback autoregulation of DDR1 expression is mediated by a DDR1-YAP/TAZ Axis, Matrix Biol 110 (2022) 129–140, https://doi.org/10.1016/j.matbio.2022.05.004.
[77] A.C. Neininger, X. Dai, Q. Liu, D.T. Burnette, The hippo pathway regulates density-dependent proliferation of IPSC-derived cardiac myocytes, Sci Rep 11 (1) (2021) 17,759, https://doi.org/10.1038/s41598-021-97,133-6.
[78] B.C. Heng, X. Zhang, D. Aubel, Y. Bai, X. Li, Y. Wei, M. Fussenegger, X. Deng, Role of YAP/TAZ in cell lineage fate determination and related signaling pathways, Front Cell Dev Biol 8 (2020) 735, https://doi.org/10.3389/fcell.2020.00735.
[79] S. Dupont, Regulation of YAP/TAZ activity by mechanical cues: an experimental overview, Methods Mol Biol 1893 (2019) 183–202, https://doi.org/10.1007/978-1-4939-8910-2_15.
[80] D. Mosqueira, S. Pagliari, K. Uto, M. Ebara, S. Romanazzo, C. Escobedo-Lucea, J. Nakanishi, A. Taniguchi, O. Franzese, P. Di Nardo, M.J. Goumans, E. Traversa, P. Pinto-do-Ó, T. Aoyagi, G. Forte, Hippo pathway effectors control cardiac progenitor cell fate by acting as dynamic sensors of substrate mechanics and nanostructure, ACS Nano 8 (3) (2014) 2033–2047, https://doi.org/10.1021/nn4058984.
[81] X. Wang, K. Zhang, L. Yang, S. Wan, Y. Liu, YAP Down-Regulated Its Target CTGF to Maintain Stem Cell Pluripotency in Human Ovarian Cancer Stem-like Cells vol. 9, 2016, pp. 6210–6216.
[82] A.A. Hartman, S.M. Scalf, J. Zhang, X. Hu, X. Chen, A.E. Eastman, C. Yang, S. Guo, YAP non-cell-autonomously promotes pluripotency induction in mouse cells, Stem Cell Reports 14 (4) (2020) 730–743, https://doi.org/10.1016/j.stemcr.2020.03.006.
[83] X. Zhou, J.P. Chadarevian, B. Ruiz, Q.-L. Ying, Cytoplasmic and nuclear TAZ exert distinct functions in regulating primed pluripotency, Stem Cell Reports 9 (3) (2017) 732–741, https://doi.org/10.1016/j.stemcr.2017.07.019.
[84] X. Varelas, R. Sakuma, P. Samavarchi-Tehrani, R. Peerani, B.M. Rao, J. Dembowy, M.B. Yaffe, P.W. Zandstra, J.L. Wrana, TAZ controls smad nucleocytoplasmic shuttling and regulates human embryonic stem-cell self-renewal, Nat Cell Biol 10 (7) (2008) 837–848, https://doi.org/10.1038/ncb1748.
[85] C. Hsiao, M. Lampe, S. Nillasithanukroh, W. Han, X. Lian, S.P. Palecek, Human pluripotent stem cell culture density modulates YAP signaling, Biotechnol J 11 (5) (2016) 662–675, https://doi.org/10.1002/biot.201500374.
[86] Musah, S.; Wrighton, P. J.; Zaltsman, Y.; Zhong, X.; Zorn, S.; Parlato, M. B.; Hsiao, C.; Palecek, S. P.; Chang, Q.; Murphy, W. L.; Kiessling, L. L. Substratum-induced differentiation of human pluripotent stem cells reveals the coactivator YAP is a potent regulator of neuronal specification. Proc Natl Acad Sci U S A 2014, 111 (38), 13,805–13,810. doi:https://doi.org/10.1073/pnas.1415330111.
[87] A. Armiñán, C. Gandía, M. Bartual, J.M. García-Verdugo, E. Lledó, V. Mirabet, M. Llop, J. Barea, J.A. Montero, P. Sepúlveda, Cardiac differentiation is driven by NKX2.5 and GATA4 nuclear translocation in tissue-specific mesenchymal stem cells, Stem Cells Dev 18 (6) (2009) 907–918, https://doi.org/10.1089/scd.2008.0292.
[88] T. Oka, M. Maillet, A.J. Watt, R.J. Schwartz, B.J. Aronow, S.A. Duncan, J. D. Molkentin, Cardiac-specific deletion of Gata4 reveals its requirement for hypertrophy, compensation, and myocyte viability, Circ Res 98 (6) (2006) 837–845, https://doi.org/10.1161/01.RES.0000215985.18538.c4.
[89] A.N. Behrens, M. Iacovino, J.L. Lohr, Y. Ren, C. Zierold, R.P. Harvey, M. Kyba, D. J. Garry, C.M. Martin, Nkx2–5 mediates differential cardiac differentiation through interaction with Hoxa10, Stem Cells Dev 22 (15) (2013) 2211–2220, https://doi.org/10.1089/scd.2012.0611.
[90] A.J. Velasquez-Mao, C.J.M. Tsao, M.N. Monroe, X. Legras, B. Bissig-Choisat, K.-D. Bissig, R. Ruano, J.G. Jacot, Differentiation of spontaneously contracting cardiomyocytes from non-virally reprogrammed human amniotic fluid stem cells, PLoS One 12 (5) (2017), e0177824, https://doi.org/10.1371/journal.pone.0177824.
[91] Y. Guo, W.T. Pu, Cardiomyocyte maturation: new phase in development, Circ Res 126 (8) (2020) 1086–1106, https://doi.org/10.1161/CIRCRESAHA.119.315862.
[92] M.M. Mia, M.K. Singh, The hippo signaling pathway in cardiac development and diseases, Front Cell Dev Biol 7 (2019) 211, https://doi.org/10.3389/fcell.2019.00211.